Geochemistry, Geophysics, Geosystems

RESEARCH ARTICLE
10.1029/2018GC007840

# Formation of the Iberian-European Convergent Plate Boundary Fault and Its Effect on Intraplate Deformation in Central Europe

**Armin Dielforder[1,2], Gianluca Frasca[2,3], Sascha Brune[1,4], and Mary Ford[2,5]**

[1]Helmholtz Centre Potsdam, GFZ German Research Centre for Geosciences, Potsdam, Germany, [2]Centre de Recherches Pétrographiques et Géochimiques, Vandœuvre-lès-Nancy, France, [3]IPGS, EOST-CNRS, Université de Strasbourg, Strasbourg, France, [4]Institute of Geosciences, University of Potsdam, Potsdam-Golm, Germany, [5]Université de Lorraine, École nationale supérieure de géologie, Vandœuvre-lès-Nancy, France

**Abstract** With the Late Cretaceous onset of Africa-Iberia-Europe convergence Central Europe experienced a pulse of intraplate shortening lasting some 15–20 Myr. This deformation event documents area-wide deviatoric compression of Europe and has been interpreted as a far-field response to Africa-Iberia-Europe convergence. However, the factors that governed the compression of Europe and conditioned the transient character of the deformation event have remained unclear. Based on mechanical considerations, numerical simulations, and geological reconstructions, we examine how the dynamics of intraplate deformation were governed by the formation of a convergent plate boundary fault between Iberia and Europe. During the Late Cretaceous, plate convergence was accommodated by the inversion of a young hyperextended rift system separating Iberia from Europe. Our analysis shows that the strength of the lithosphere beneath this rift was initially sufficient to transmit large compressive stresses far into Europe, though the lithosphere beneath the rift was thinned and thermally weakened. Continued convergence forced the formation of the plate boundary fault between Iberia and Europe. The fault evolved progressively and constituted a lithospheric-scale structure at the southern margin of Europe that weakened rheologically. This development caused a decrease in mechanical coupling between Iberia and Europe and a reduction of compressional far field stresses, which eventually terminated intraplate deformation in Central Europe. Taken together, our findings suggest that the Late Cretaceous intraplate deformation event records a high force transient that relates to the earliest strength evolution of a lithospheric-scale plate boundary fault.

**Key Points:**
- Late Cretaceous Iberia-Europe convergence caused the formation of a convergent plate boundary fault between the continents
- The rheological strength of the fault governed plate coupling and the transmission of compressive stress into Europe
- Initially strong plate coupling drove deformation in Europe, which ceased after ~15–20 Myr due to a weakening of the fault

**Supporting Information:**
- Supporting Information S1

**Correspondence to:**
A. Dielforder,
armin.dielforder@gfz-potsdam.de

**Citation:**
Dielforder, A., Frasca, G., Brune, S., & Ford, M. (2019). Formation of the Iberian-European convergent plate boundary fault and its effect on intraplate deformation in Central Europe. *Geochemistry, Geophysics, Geosystems*, *20*, 2395–2417. https://doi.org/10.1029/2018GC007840

Received 19 JUL 2018
Accepted 18 APR 2019
Accepted article online 3 MAY 2019
Published online 24 MAY 2019



## 1. Introduction

Forces acting along tectonic plate boundaries induce horizontal stress in the interior of continents. Modern stress data indicate that plate boundary compression can control the direction of the maximum horizontal compressive stress far away from plate boundaries, even though the stress state may switch from deviatoric compression to deviatoric tension within a few hundreds of kilometers (Heidbach et al., 2007; Levandowski et al., 2018; Zoback, 1992; Zoback & Zoback, 1989). Such changes in stress state indicate that the magnitude of the induced stress decreases and that the stress field becomes controlled by a superposition of far-field stress and local stress arising, for example, from variations in the gravitational potential energy (Jones et al., 1996; Levandowski et al., 2018). However, occasionally plate boundary compression can cause deviatoric compression over large areas within continental interiors. The compression can be strong enough to drive deformation within regions of reduced lithospheric strength, as manifested by the inversion of intracontinental rift basins, uplift of basement blocks, or intracontinental orogeny (Dyksterhuis & Müller, 2008; Raimondo et al., 2014; Turner & Williams, 2004; Ziegler, 1987; Ziegler et al., 1995). In this sense, ancient intraplate deformation events provide a record of geological periods, during which continental interiors experienced regional deviatoric compression. Linking such events to their geodynamic causes can help to better understand the factors that allow enhanced plate boundary compression and how they evolve through time.

In this context, we investigate the causes of a short-lived intraplate deformation event affecting Central Europe in Late Cretaceous time. The deformation event has previously been interpreted as a far-field response to plate convergence between Africa, Iberia, and Europe, but the factors controlling the timing and duration of deformation have remained open to debate (Dèzes et al., 2004; Kley & Voigt, 2008; Nielsen et al., 2007; Ziegler et al., 1995). We here propose that the dynamics of Late Cretaceous intraplate

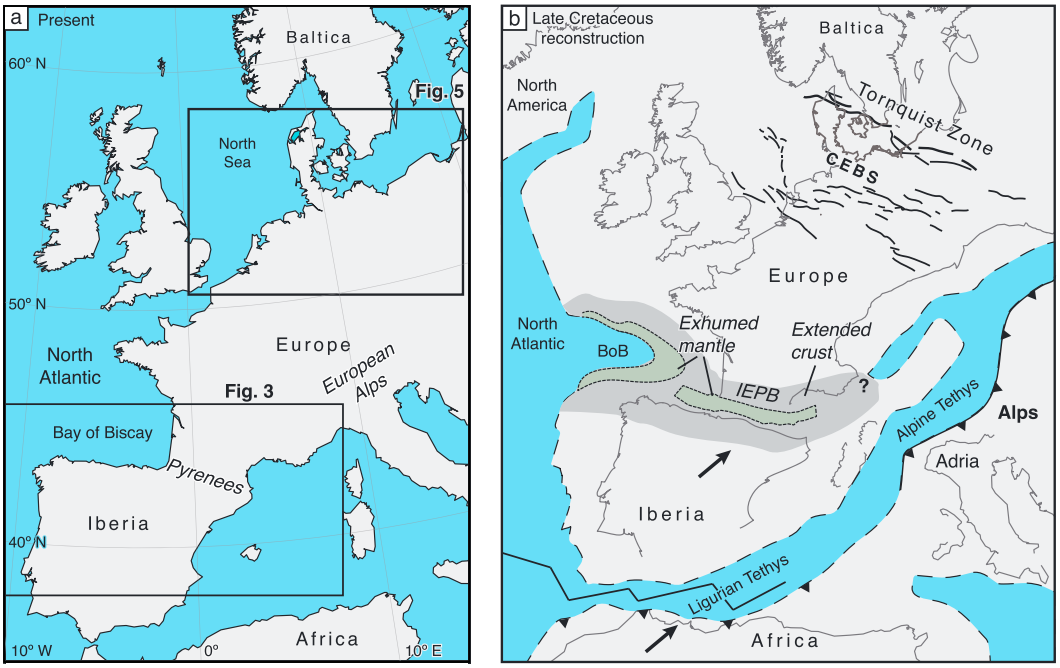


**Figure 1.** Geographic overview. (a) Present-day geographic map of Europe showing the location of the two study areas. (b) Paleogeographic reconstruction of Europe during the Late Cretaceous. Based on Kley and Voigt (2008), Macchiavelli et al. (2017), Rosenbaum et al. (2002), and Tugend et al. (2015). Black arrows indicate the direction of Africa-Iberia and Iberia-Europe convergence during the Late Cretaceous. IEPB = Iberian European plate boundary. CEBS = Central European Basin System (black lines are major faults). Green and dark gray areas indicate zones of exhumed mantle rocks and extended continental crust, respectively, in the Pyrenean realm and Bay of Biscay (BoB). Light gray and blue areas indicate continental and oceanic domains, respectively. Baltica refers to the Proterozoic continent that constitutes the northwestern part of western Eurasia ("Europe"). Europe became welded to Baltica during the Caledonian and Variscan orogenies. The Tornquist zone is part of the Paleozoic suture between Baltica and Europe.

deformation were governed by the formation and rheological evolution of a convergent plate boundary fault between Iberia and Europe, which marked the earliest stages of Pyrenean orogeny. In the following, we first review geological constraints on the Late Cretaceous to Eocene tectonics in the Pyrenean realm and in Central Europe and discuss previous explanations of the intraplate deformation event in Europe. Subsequently, we analyze how the deviatoric compression of Central Europe depended on the formation and rheological evolution of a convergent plate boundary fault between Iberia and Europe. The plausibility of our analysis is evaluated by numerical simulations. We close with a discussion of our findings, in which we address differences in the tectonic setting along-strike the Iberian-European plate boundary as well as possible implications for the earliest tectonics in the Pyrenees.

## 2. Geological Background

### 2.1. Plate Tectonic Framework

Plate convergence between Africa, Iberia, and Europe commenced in the Late Cretaceous around 84 Ma (e.g., Macchiavelli et al., 2017; Rosenbaum et al., 2002). At this time, Africa and Iberia were separated by the Ligurian Tethys that connected the Alpine Tethys to the east and the Atlantic Ocean to the west (Figure 1; Handy et al., 2010; Macchiavelli et al., 2017). Iberia and Europe were separated by a hyperextended rift system and the Bay of Biscay, a narrow oceanic basin in the west (Clerc et al., 2012; Nirrengarten et al., 2018; Roca et al., 2011; Tugend et al., 2014). The oceanic domains and the rift system had previously formed in response to oblique divergence between Africa and Europe, mainly in Jurassic to Early Cretaceous times (e.g. Schettino & Turco, 2011). From the Late Cretaceous onward, approximately NE directed plate convergence was accommodated both, between Africa and Iberia and between Iberia and Europe. Convergence between Iberia and Europe was accommodated along a plate boundary that extended

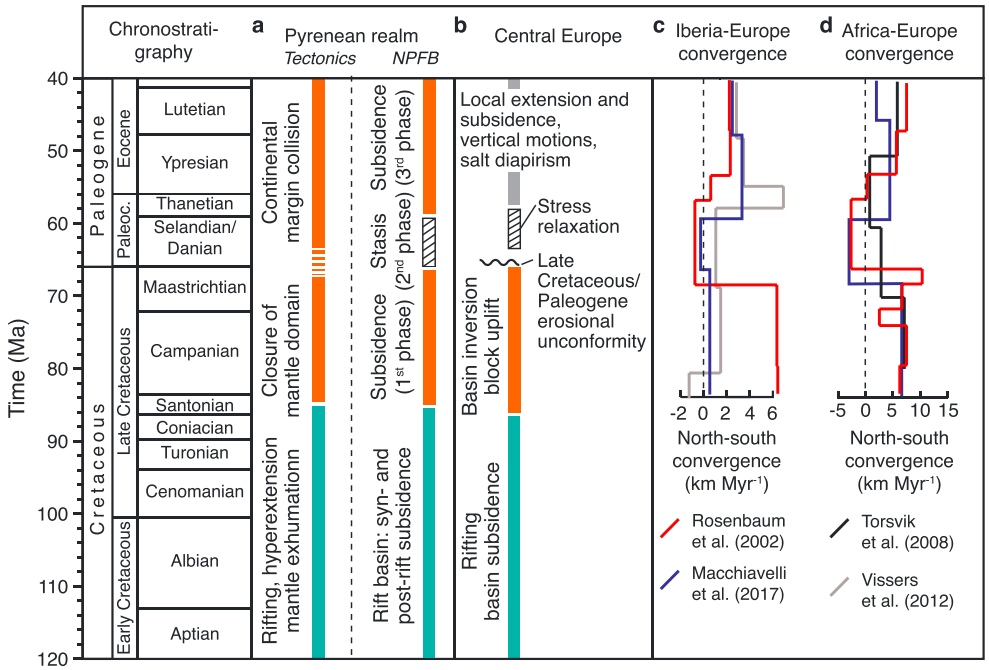


**Figure 2.** Correlation of geological events. (a) Tectonic evolution in the Pyrenean realm and subsidence phases in the North Pyrenean Foreland Basin (NPFB). (b) Rifting and inversion tectonics in Central Europe. (c, d) North-south convergence rates between Iberia-Europe and Africa-Europe following different plate kinematic reconstructions. See text for details and references.

at least from the Bay of Biscay area to the eastern Pyrenees and potentially continued into the Alpine realm (Macchiavelli et al., 2017; Vissers & Meijer, 2012). Convergence between Africa and Iberia is thought to have been accommodated by slow subduction of the Ligurian Tethys beneath Africa (e.g., Vergés & Fernàndez, 2012).

Some plate kinematic reconstructions suggest that the motion between Africa-Iberia-Europe changed at the transition from the Late Cretaceous to the Paleocene (Macchiavelli et al., 2017; Rosenbaum et al., 2002; Schettino & Turco, 2011). In detail, approximately NE directed plate convergence switched to left-lateral and subsequent right-lateral strike slip movements. Simultaneously, Africa moved slightly southward relative to Iberia. The rearrangement of the convergence direction caused a slowdown or break in north directed convergence during the Paleocene (Figures 2c and 2d). In the late Paleocene, north directed convergence between Africa-Iberia and Iberia-Europe restarted. Convergence was accommodated along the Iberian-European plate boundary (IEPB) until the early Miocene. After this, the convergence between Africa and Europe was accommodated in the Ligurian Tethys domain further south (e.g., Frasca et al., 2015; Macchiavelli et al., 2017).

### 2.2. Pyrenees

The Pyrenees are a collisional orogen resulting from the Late Cretaceous to Miocene convergence between Iberia and Europe (Muñoz, 1992; Roure et al., 1989; Vergés et al., 1995). The orogen strikes WNW-ESE and shows a double vergent geometry, with a south vergent pro-wedge developed on the lower plate (Iberia) and a north vergent retro-wedge situated on the upper plate (Europe; Figures 3 and 4a). The pro-wedge and retro-wedge are separated along the North Pyrenean Fault, which is classically interpreted as the suture between Iberia and Europe (Figure 4a; Choukroune & Mattauer, 1978). This structural configuration developed during the main phase of continental collision, which commenced during the late Paleocene and was largely characterized by the northward subduction of Iberian lower crust and mantle lithosphere, the southward accretion and backthrusting of Iberian Paleozoic basement units (Axial Zone), the propagation of the southern foreland fold and thrust belt, and minor north directed shortening in the retro-wedge (Beaumont et al., 2000; Chevrot et al., 2015; Grool et al., 2018; Mouthereau et al., 2014; Vergés et al., 2002). Prior to the onset of

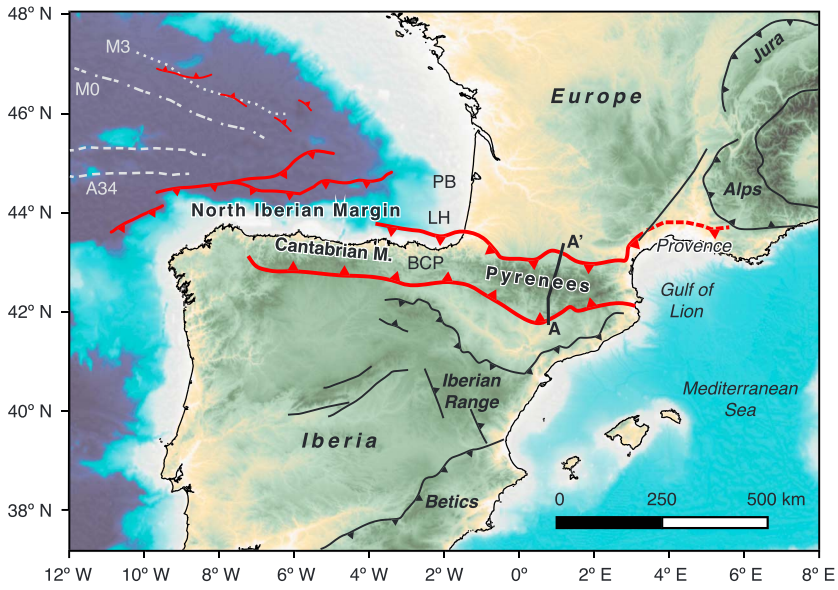


**Figure 3.** Tectonic framework of Iberia. Red thrust faults indicate frontal thrust systems related to the Pyrenean orogeny. Black thrust faults indicate thrust systems belonging to other orogenic events. Magnetic anomalies in the Bay of Biscay (M3, M0, A34) from Sibuet et al. (2004). Thick black line indicates the trace of cross section A-A′ shown in Figure 4a. PB, Parentis Basin; LH, Landes High; BCP, Basque-Cantabrian Basin.

collision, that is, during the early phase of plate convergence from the Late Cretaceous to Paleocene, the evolution of the Pyrenean realm was largely characterized by the inversion of the hyperextended rift system located between Iberia and Europe (Figure 4b). In the following, we focus on the precollisional to early

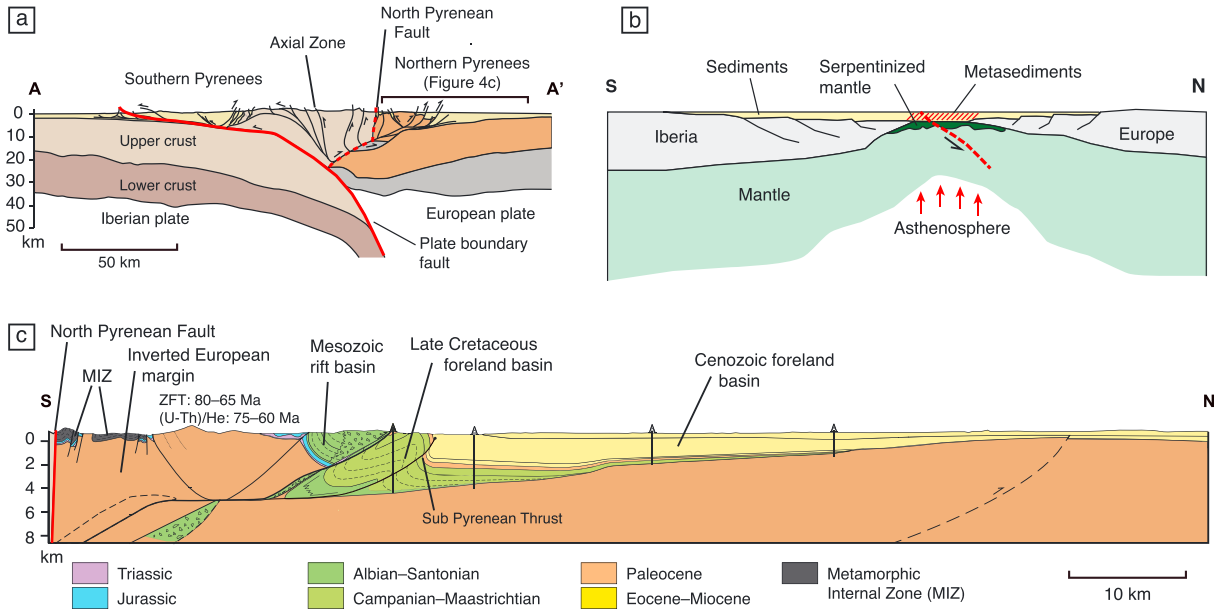


**Figure 4.** Geological information for the Pyrenees. (a) Simplified interpretation of the ECORS Pyrenees deep seismic section across the central Pyrenees. Modified after Muñoz (1992). (b) Schematic reconstruction of the preorogenic template, shortly before the onset of plate convergence. A hyperextended rift system separates Iberia and Europe. Mantle rocks are exhumed and serpentinized in the rift center. Sediments deposited on the exhumed mantle experience high temperature-low pressure metamorphism. The metasediments are later thrust onto the European margin (MIZ in Figure 4c). Dashed red line indicates the plate boundary fault that develops with the onset of plate convergence. Based on Clerc et al. (2015), Grool et al. (2018), and Mouthereau et al. (2014). (c) Balanced geological cross section through the Northern Pyrenees along the ECORS Pyrenees transect. Modified after Ford et al. (2016). Zircon fission track ages (ZFT) and Zircon (U-Th)/He ages from Yelland (1991) and Ternois et al. (2019), respectively.

collisional evolution of the Pyrenees and summarize key information that provides insights into the tectonics around the onset of Africa-Iberia-Europe convergence. For further information on the Pyrenean orogeny we refer to the recent literature (Angrand et al., 2018; Grool et al., 2018; Labaume et al., 2016; Mouthereau et al., 2014; Teixell et al., 2018; Tugend et al., 2014; Vacherat et al., 2017).

Rifting between Iberia and Europe began already in the Triassic with the main phase of extension during the Early Cretaceous (Figure 2a). Hyperextension culminated in limited crustal breakup and exhumation of subcontinental mantle within a narrow, few tens of kilometer-wide domain (Figure 4b; Clerc et al., 2012; Lagabrielle et al., 2010; Masini et al., 2014; Mouthereau et al., 2014; Roca et al., 2011; Tugend et al., 2015). Remnants of exhumed mantle rocks, together with some intrusive and effusive magmatic rocks, are preserved within strongly deformed metasediments that crop out in a narrow zone, just north of the North Pyrenean Fault (Metamorphic Internal Zone in Figure 4c). These sediments experienced high temperature-low pressure metamorphism in between ~110 and 90 Ma (Albian to Turonian), during which temperatures of ~400–600 °C were reached (Clerc & Lagabrielle, 2014; de Saint Blanquat et al., 1990, 2016; Vacherat et al., 2014). The metasediments are thought to have been deposited within the exhumed mantle domain, where they were metamorphosed soon after deposition (Figure 4b; e.g., Clerc et al., 2015). Restored geological cross sections from the central to eastern Pyrenees suggest that the metasediments were subsequently sheared off the mantle domain and thrust onto the southernmost rifted margin of Europe during early stages of Africa-Iberia-Europe convergence (Clerc et al., 2016; Ford et al., 2016; Grool et al., 2018). The preservation of the Metamorphic Internal Zone above the inverted margin of Europe just north of the North Pyrenean Fault and its absence south of the fault indicates that the IEPB fault that accommodated convergence between Iberia and Europe and enabled the closure of the mantle domain initiated somewhere south of the European margin, presumably within the mantle domain (Figure 4b; Grool et al., 2018; Mouthereau et al., 2014; Tugend et al., 2014). The North Pyrenean Fault represents possibly a remnant of the initial plate boundary fault, but the temporal and structural development of this fault is still poorly understood. At present, the North Pyrenean Fault is subvertical and is thought to terminate at depths against a deeper fault system (Figure 4a; Choukroune & ECORS-Pyrenees-Team, 1989).

Details of the earliest phase of rift inversion in response to plate convergence are preserved in the Northern and Southern Pyrenees. In the South Pyrenean fold and thrust belt the inversion of rift-inherited normal faults is recorded by syntectonic Upper Santonian to Maastrichtian growth strata, indicating that the inversion started no later than ~84 Ma (McClay et al., 2004). A similar timing is provided by the synsedimentary propagation of thrust faults into Campanian and Maastrichtian sediments deposited in the South Pyrenean foreland (Ardévol et al., 2000). In the Northern Pyrenees, the timing of rift inversion is recorded by the development of the North Pyrenean foreland basin (NPFB) that developed as a retro-wedge basin on the extended southern margin of Europe (Figure 4c). In the central to eastern Pyrenees, the basin comprises a ~3- to 5-km-thick succession of Upper Cretaceous to Miocene synorogenic sediments. The succession records a switch from slow, postrift thermal subsidence to increased subsidence around 84 Ma (Ford et al., 2016; Grool et al., 2018; Rougier et al., 2016). Sequentially restored cross sections indicate that the NPFB developed in front of basement blocks that were inverting along rift-inherited normal faults (Figure 4c; Ford et al., 2016; Grool et al., 2018; Rougier et al., 2016). The Late Cretaceous inversion of basement blocks is recorded by zircon fission track ages and zircon (U-Th)/He ages recording exhumation related cooling of the basement blocks around ~80–65 and ~75–60 Ma, respectively (Figure 4c; Ternois et al., 2019; Yelland, 1991).

Most geological reconstructions propose that by the end of the Cretaceous, the exhumed mantle domain was closed and Iberia had begun to thrust beneath Europe (Ford et al., 2016; Grool et al., 2018; Mouthereau et al., 2014). The timing is consistent with potassium feldspar $^{40}Ar/^{39}Ar$ multiple diffusion domain thermal models that indicate the onset of heating of the distal Iberian margin around 65 Ma (Metcalf et al., 2009). In the subsequent collisional phase, plate convergence was mainly accommodated within the pro-wedge, while the retro-wedge experienced only limited shortening (Beaumont et al., 2000; Ford et al., 2016; Grool et al., 2018).

### 2.3. Central Europe

Central Europe experienced repeated phases of intraplate rifting throughout the late Paleozoic and Mesozoic leading to the formation of several basins, which are commonly grouped into the Central European Basin System (CEBS; Figures 2b and 5a). The three largest subbasins are the Norwegian-Danish Basin, the North German Basin, and the Polish Basin (Figures 1 and 5a). These basins accommodated up to ~6,000–

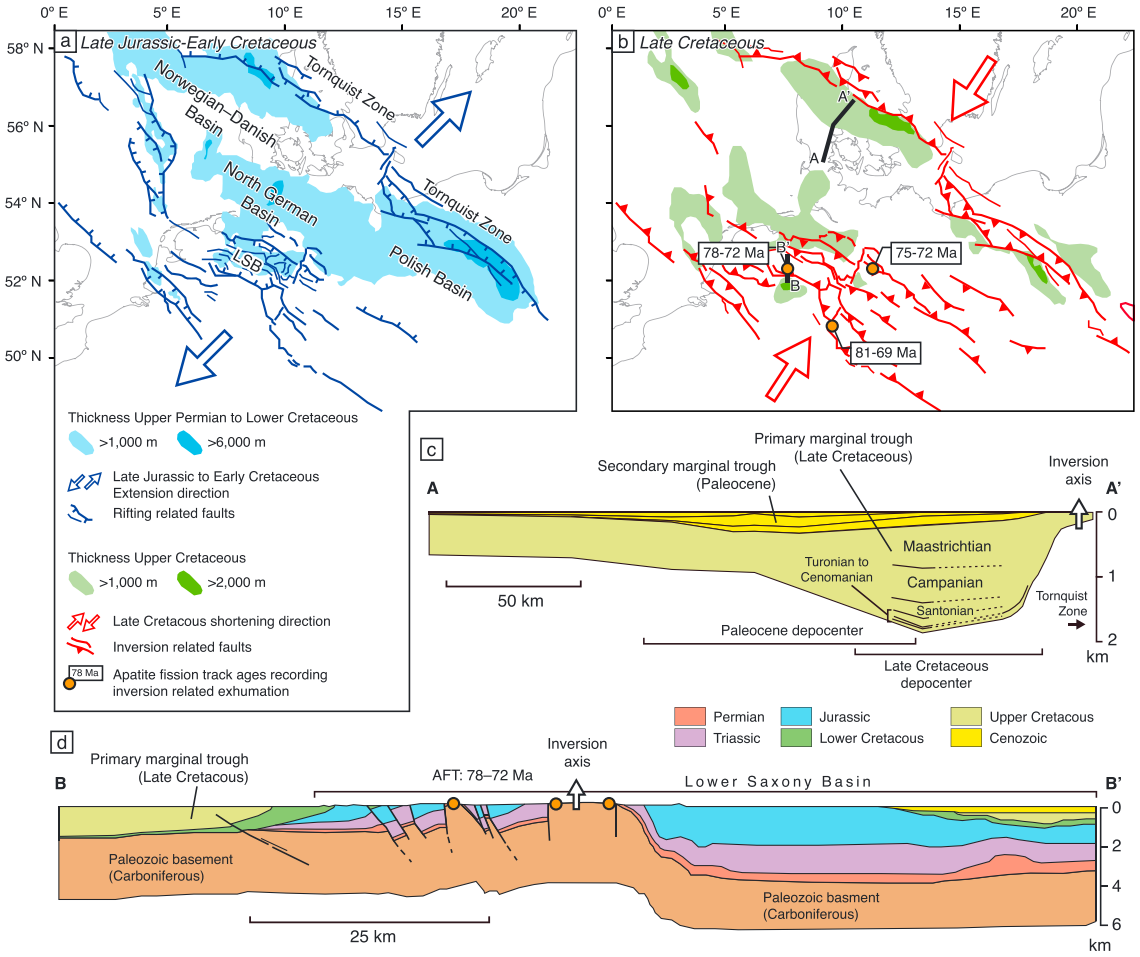


**Figure 5.** Geological information for the Central European Basin System. (a, b) Maps showing the main depocenters and main structures active during (a) Late Jurassic-Early Cretaceous rifting, and (b) during Late Cretaceous basin inversion. LSB = Lower Saxony Basin. Black lines in (b) indicate the traces of cross sections shown in Figure 5c (A-A′) and in Figure 5d (B-B′). Based on Kley et al. (2008) and Scheck-Wenderoth and Lamarche (2005). Apatite fission track ages (orange circles) from Thomson and Zeh (2000), Senglaub et al. (2005), and Fischer et al. (2012). (c) Cross section through the primary and secondary marginal trough formed during inversion of the Norwegian-Danish Basin. Modified from Nielsen et al. (2005). (d) Cross section through the southern margin of the Lower Saxony Basin. Modified from (Senglaub et al., 2005).

8,000 m of sediments within their depocenters (Scheck-Wenderoth & Lamarche, 2005). During the Late Jurassic to Early Cretaceous, Central Europe experienced approximately NE-SW directed extension, which was followed by a phase of NNE-SSW directed shortening in the Late Cretaceous, recording a change in the regional stress field from deviatoric tension to deviatoric compression (Figures 2b and 5b; Kley & Voigt, 2008; Navabpour et al., 2017; Sippel et al., 2009). Intraplate shortening was largely accommodated along rift-inherited, NW-SE trending normal faults and caused the inversion and exhumation of Mesozoic basins and Paleozoic basement blocks, such as the Bohemian Massif and the Harz Mountains (Kley & Voigt, 2008; Navabpour et al., 2017; Tanner & Krawczyk, 2017; von Eynatten et al., 2008). The inversion was essentially thick-skinned but involved also thin-skinned thrusting along detachments developed in Permian and Triassic evaporates (Kockel, 2003; Lohr et al., 2007; Tanner & Krawczyk, 2017; Ziegler, 1987). The magnitude of exhumation varies across the CEBS with an average of around a few thousand meters (~1,000–4,000 m), but reaching up to ~7,000 m in the Lower Saxony subbasin at the southern margin of the North German Basin (Figures 5b and 5d; Littke et al., 2008; Senglaub et al., 2005, 2006). In front of the inversion zones, new basins, so-called marginal troughs, were syntectonically infilled with up to ~2,000 m of sediment (Figure 5c; Scheck-Wenderoth & Lamarche, 2005). The syntectonic sedimentary record of the marginal troughs suggests that the main phase of inversion occurred during Late Santonian and Campanian. The timing is consistent with apatite fission track data from the CEBS, which is interpreted to record exhumation

related cooling during the Campanian (apatite fission track ages of ~81–69 Ma; Fischer et al., 2012; Senglaub et al., 2005; Thomson & Zeh, 2000).

Intraplate deformation ceased around the end of the Late Cretaceous, that is, after only ~15–20 million years, which is well recorded by the sealing of eroded inversion structure by Maastrichtian or early Paleogene sediments (Kley et al., 2008; Kley & Voigt, 2008; Lohr et al., 2007; Scheck-Wenderoth & Lamarche, 2005). During the Paleocene, some areas of the CEBS experienced dome-like uplift without reactivation of faults. Likewise, depocenters were shifted outward, causing the formation of secondary marginal troughs, partly overlapping the earlier marginal troughs (Figure 5c). Vertical displacements were rather small, in the order of a few hundred meters (de Jager, 2003; Deckers, 2015; Nielsen et al., 2005). Based on numerical simulations of basin inversion, the Paleocene vertical displacements have been explained as a stress relaxation feature related to the mechanical unloading of the lithosphere, suggesting that both the contraction and the horizontal deviatoric compression of Central Europe ended during the early Paleocene (Nielsen et al., 2005, 2007).

After the Paleocene, the kinematics and stress conditions in Central Europe became more heterogeneous. From the Eocene to Miocene the European Cenozoic Rift System opened, which records W-E to NW-SE directed extension (e.g., Dèzes et al., 2004; Schumacher, 2002). At approximately the same time, minor compressive deformation occurred in the southern North Sea and the English Channel (de Lugt et al., 2003; Ziegler et al., 1995). In the CEBS local salt diapirism and extensional faulting is recorded. From around Middle Miocene onward, Central Europe experienced NW-SE directed compression in response to continental collision in the European Alps (Bourgeois et al., 2007; Kley & Voigt, 2008; Navabpour et al., 2017).

## 3. Previous Explanations for Intraplate Deformation in Central Europe and Open Questions

Ziegler (1987) and Ziegler et al. (1995) interpreted the Late Cretaceous intraplate deformation in Central Europe to reflect collisional plate interaction related to the Alpine orogeny. Although occasionally questioned (e.g., Dewey & Windley, 1988; Vejbæk & Andersen, 2002), the concepts of Ziegler (1987) and Ziegler et al. (1995) have been widely accepted and adopted in the literature (Dèzes et al., 2004; Krzywiec, 2006; Marotta et al., 2002; Nielsen et al., 2005). More recently, Kley and Voigt (2008) reconsidered the linkage between Late Cretaceous intraplate deformation and the Alpine orogeny. Based on new structural and kinematic data from the European inversion zones and the Alpine realm, the authors show that neither the timing nor the shortening directions in Central Europe are compatible with the Late Cretaceous tectonics in the Alpine realm. In particular, when Europe experienced NNE directed contraction, the Alpine orogen was undergoing a phase of NW directed extension, probably related to subduction erosion (Bachmann et al., 2009; Wagreich, 1995). Moreover, the orogen was still separated from the European margin by the Alpine Tethys (Figure 1b) and there is no evidence for Late Cretaceous shortening within the future European foreland, except for some localities in southern France, which is incompatible with the transfer of large compressive stresses into the Alpine foreland (Handy et al., 2010; Kley & Voigt, 2008; Pfiffner et al., 2002).

Kley and Voigt (2008) point out that both the timing and kinematics of intraplate deformation are consistent with the onset of NE directed Africa-Iberia-Europe convergence around 84 Ma (Figure 2). The authors note that about the same time N to NE directed shortening in the Moroccan High Atlas (North Africa) commenced. Likewise, Mesozoic basins at the southern margin of Iberia experienced a phase of accelerated subsidence, probably in response to tectonic shortening between Iberia and Africa (Froitzheim et al., 1988; Reicherter & Pletsch, 2000; Vergés & Fernàndez, 2012). Kley and Voigt (2008) therefore suggest that at the onset of NE directed plate convergence, the relatively thin and weak lithosphere of Iberia and Europe became pinched between the stronger cratonic lithosphere of Africa and Baltica causing distributed deformation across Iberia and Europe including deformation within the Pyrenean realm.

The termination of intraplate deformation has been linked to the Paleocene interruption of north directed Africa-Iberia-Europe convergence (Figures 2c and 2d; Kley & Voigt, 2008; Nielsen et al., 2007). At present, the exact nature of this interruption is not clear. For example, some plate kinematic reconstructions indicate only a slowdown of plate convergence, rather than a full stop or even extension (Figures 2c and 2d; Torsvik et al., 2008; Vissers & Meijer, 2012). Other reconstructions that show the interruption suggest strike slip motions between Iberia and Europe during the Paleocene (section 2.1), but conclusive field data from the Pyrenees that confirm such motions are still lacking. Independently, if intraplate deformation is

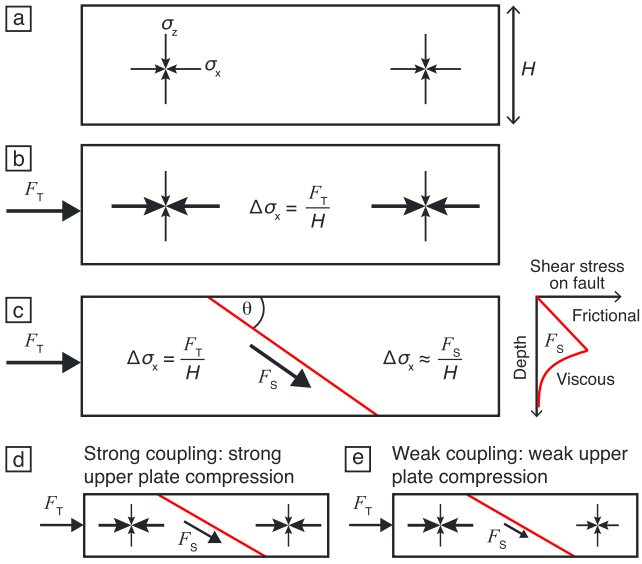


**Figure 6.** Sketch illustrating the concept of plate coupling. $\sigma_x$ and $\sigma_z$ are the horizontal stress and vertical stress, respectively. $F_T$ is a tectonic force laterally applied to a lithosphere of thickness $H$. $\Delta\sigma_x$ is the average differential stress resulting from the force $F_T$. $F_S$ is the plate coupling force and, that is, the integrated shear stress along the fault dipping at angle $\theta$. See text for details.

understood merely as the effect of plate convergence, the possible interruption of convergence provides a feasible explanation for the termination of intraplate shortening. However, from this understanding, the question arises, why shortening did not continue when convergence restarted at the end of the Paleocene? In addition, the Late Eocene to Miocene development of the European Cenozoic Rift System document that large parts of Europe experienced deviatoric tension during the Cenozoic phase of Africa-Iberia-Europe convergence. In contrast, the Pyrenean orogeny continued until the Miocene and Iberia also experienced intraplate shortening during the Cenozoic, for example, in the Iberian Range south of the Pyrenees (Figure 3; Guimerà et al., 2004; Sainz & Faccenna, 2001). The picture that emerges is that Central Europe responded very differently to north directed Africa-Iberia-Europe convergence during Late Cretaceous and Cenozoic time. In the following we present a possible explanation for the inferred dynamics.

## 4. Intraplate Deformation and Plate Coupling Along the Iberian European Convergent Plate Boundary Fault

### 4.1. Effect of Plate Coupling

The consistency in the kinematics and timing of intraplate deformation and the onset Africa-Iberia-Europe convergence (Figure 2) suggests that intraplate deformation was driven by plate boundary compression. Thereto, the force driving plate convergence must have induced large compressive stresses into the interior of Europe. The magnitude of the compressive stress that is induced into a continent depends strongly on the mechanical strength of the plate boundary fault, that is, the main fault system that constitutes the interface between two converging plates and accommodates the convergence at the lithospheric scale (Molnar & England, 1990; Wang & He, 1999). To illustrate this dependence, we first consider a laterally confined, elastic lithosphere of thickness $H$ that is at the lithostatic reference state of stress, that is, $\sigma_x = \sigma_z = \rho g z$, where $\rho$ is the average rock density, $g$ the gravitational acceleration, and $z$ is depth (Figure 6a). If a tectonic force $F_T$ is laterally applied from one side, the lithosphere is set everywhere under horizontal deviatoric compression, where the average differential stress $\Delta\sigma_x$ equals $F_T/H$ (Figure 6b). For $F_T = 4 \times 10^{12}$ N/m and $H = 80$ km, $\Delta\sigma_x$ is 50 MPa. At convergent plate margins there is no continuous lithosphere, but two lithospheres that are mechanically coupled along the plate boundary fault dipping at angle $\theta$ (Figure 6c). The intensity of coupling depends on the plate coupling force $F_S$, which is the depth-integrated static shear stress along the fault (Wang & He, 1999). The magnitude of $F_S$ is therefore directly related to the rheological strength of the fault. The plate coupling force causes horizontal deviatoric compression of the upper plate, where the differential stress away from the plate boundary fault is $\Delta\sigma_x \approx F_S/H$ (Wang & He, 1999). If $F_S$ approaches $F_T$, then the deviatoric compression in the upper plate and the lower plate are similar and it can be said that the plates are strongly coupled. In other words, $F_T$ is effectively transmitted into the upper plate (Figure 6d). If $F_S \ll F_T$, then the deviatoric compression in the upper plate is less than in the lower plate and the plates are weakly coupled (Figure 6e). Thus, only a fraction of $F_T$ is transmitted into the upper plate. We note that the plate coupling force resists plate convergence (van den Beukel, 1992). If $F_T$ is the force driving plate convergence, for example, the push a distant ridge, then plate convergence would stop if $F_S = F_T \cos\theta$, because the resistance force equals the driving force. If $F_S < F_T \cos\theta$, then the difference between the two drives the underthrusting or subduction of the lower plate.

The above considerations do not provide a full force balance for convergent plate margins and allow only a first-order estimate of the stress conditions in the upper plate. In particular, the presence of a high mountain belt affects the stress state in the upper plate, because the gravitational force in the presence of topography creates deviatoric tension (e.g., Lamb, 2006; Wang & He, 1999). Nevertheless, the concept of plate coupling describes an elementary relation between $F_S$ and upper plate compression that is of direct relevance for the dynamics of intraplate deformation in Central Europe, as addressed in the following.

The intraplate deformation event indicates that the force driving Africa-Iberia-Europe convergence was effectively transmitted into Europe throughout the Late Cretaceous phase of plate convergence. Likewise, the termination of intraplate deformation suggests that the transmission of the plate tectonic force into Europe ceased around the end of the Late Cretaceous. Based on the above considerations of plate coupling and taking into account that shortening in the Pyrenean realm and in the interior of Iberia continued during the Cenozoic, which documents a transfer of tectonic driving forces between Africa and Iberia after the Late Cretaceous, we propose that the inferred dynamics reflect a change in the coupling along the Iberian-European plate boundary fault. In this sense, coupling along the IEPB fault was strong enough during the Late Cretaceous to drive intraplate deformation but became insufficient afterward when intraplate deformation ceased. Given that the plate coupling force depends on the rheological strength of the plate boundary fault, we suppose that the decrease in plate coupling was related to a rheological weakening of the IEPB fault.

### 4.2. Evaluation of the Plate Coupling Force

To examine our hypothesis, we calculated $F_S$ for varying rheological configurations of the plate boundary fault considering frictional deformation and temperature-dependent viscous deformation. The calculations were performed for two different settings that approximate the thickness and thermal structure of the lithosphere beneath the hyperextended rift system around the early phase of plate convergence during Late Santonian and Campanian time (Setting I) and around the transition from the Late Cretaceous to the Paleocene (Setting II). The thickness of the lithosphere has been adopted from lithospheric-scale restorations of the central Pyrenees from Mouthereau et al. (2014). The lithospheric thicknesses are 40 and 80 km for Setting I and Setting II, respectively (Figures 7a and 7b). To approximate the thermal gradient beneath the hyperextended rift system, we fitted a geotherm through the model lithosphere (Stüwe, 2007; supporting information Table S1). Thereto, we assumed a standard temperature of 1300 °C at the lithosphere asthenosphere boundary (LAB) for both settings. For Setting I, we adjusted the thermal gradient in the upper ~10 km to ~50 °C/km (Figure 7a). The elevated thermal gradient accounts for the high-temperature metamorphism occurring in the exhumed mantle domain in between ~110 and 90 Ma, during which thermal gradients of ~40–80 °C/km persisted within the upper kilometers (section 2.2). Since plate convergence started only a few million years after the metamorphic event, we can assume that the thermal gradient was still high at the onset of convergence. For Setting II, we adjusted the thermal gradient in the upper ~10 km to ~30 °C/km (Figure 7b). The lower thermal gradient is assumed because there is little or no evidence for synorogenic metamorphism in the Pyrenees. Moreover, these constructed geotherms and the assumed lithospheric thicknesses are in agreement with numerical simulations presented below (section 4.4).

We quantify $F_S$ by means of an analytical model that computes the static shear stress along a planar fault cutting through the lithosphere. This approach implies that the fault formed a lithospheric-scale structure already at the onset of plate convergence. In reality it is more likely that the fault initiated as a new structure that evolved with ongoing plate convergence. Alternatively, the fault may have also reactivated a rift-inherited weak detachment fault, as previously suggested (e.g., Jammes et al., 2009). To consider these different possibilities, we calculate $F_S$ by accounting for varying rheological fault strengths. Thereto, we first assign a rheological strength to the fault that is identical to the pristine strength of the lithosphere, which can be understood as a fault that starts to develop and is not yet weakened. To describe the strength of the lithosphere, we distinguish between the sediments covering the rift system (upper 5 km), serpentinized mantle (5 km), and mantle lithosphere below (Figures 7a and 7b). For the sediments we assume an effective coefficient of friction ($\mu'$) of 0.24 that accounts for a normal coefficient of friction ($\mu$) of 0.6 and moderate pore fluid overpressures within the sediments (pore fluid pressure ratio $\lambda = 0.6$). To account for viscous deformation within the sediments, we adopt a wet quartz flow (Gleason & Tullis, 1995; supporting information Table S2). For the serpentinized mantle we assume $\mu' = 0.06$, which accounts for the low effective frictional strength of serpentinites and moderate pore fluid overpressures (Escartín et al., 2001; Moore et al., 1997). For the mantle lithosphere we assume $\mu = 0.6$ and a dry olivine flow law (Hirth & Kohlstedt, 2003). To simulate a weakening of the fault, we use a weak fault rheology that is given by $\mu' = 0.06$ and a wet quartz flow law for simplicity. We then vary for both settings the depth to which the fault is described by the weak fault rheology. Below this depth, the fault has a rheological strength identical to the lithosphere. This approach allows to account for a possible reactivation of a weak rift-inherited fault structure for Setting I and to mimic

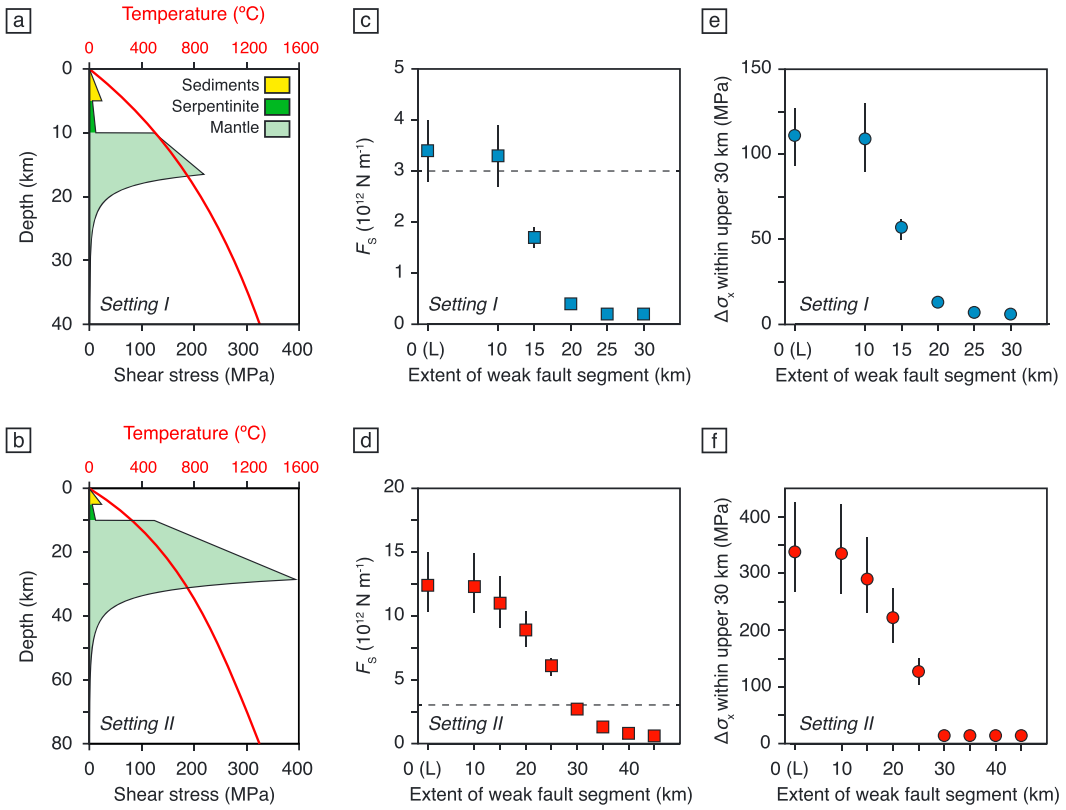


**Figure 7.** Analysis of plate coupling force $F_S$. (a, b) Shear strength envelopes for the lithosphere beneath the rift center for Setting I and Setting II, respectively. The solutions shown were obtained for a strain rate of $10^{-13}$ s$^{-1}$ and a dip angle of the fault of 30°. See text and supporting information for details on the rheological parameters. (c, d) Plate coupling force as function of depth to which the fault is characterized by a weak fault rheology. The values at 0 km indicate the shear strength of the lithosphere (L). Dashed horizontal line indicates the force required to drive intraplate deformation (e, f) Average differential stress ($\Delta\sigma_x$) induced in the upper 30 km of the upper plate as function of depth to which the fault is characterized by a weak rheology. Error bars in Figures 7c–7f account for uncertainties in the strain rate ($\pm 0.5 \times 10^{-13}$ s$^{-1}$) and dip angle of the fault (±5°).

different degrees of fault weakening for Setting II. The force $F_S$ is obtained by integrating the shear stress along the fault. Although this approach cannot reproduce the exact fault rheology, it provides a first-order estimate for the magnitude of $F_S$ and illustrates how $F_S$ varies with the rheological strength of the fault.

For Setting I, the strength of the lithosphere is $3.4 \times 10^{12}$ N/m (Figures 7a and 7c). The strength of a fault that is not yet weakened would be identical to the strength of the lithosphere. For a fault that is weakened in the upper 10 km, $F_S$ is nearly identical to the strength of the lithosphere. This is because we assigned sediments and serpentinites to the upper 10 km of the lithosphere, for which the assumed rheologies are similar to the weak fault rheology. If the fault is weakened to depths greater than 10 km, $F_S$ drops rapidly below $1 \times 10^{12}$ N/m (Figure 7c). For Setting II, the strength of the lithosphere is substantially higher with ~$12.4 \times 10^{12}$ N/m (Figures 7b and 7d). For a fault that is weakened within the upper 10–25 km, $F_S$ has comparatively high values of $6.1 \times 10^{12}$ to $12.3 \times 10^{12}$ N/m. If the fault is weakened to greater depth, $F_S$ decreases rapidly to values $<1 \times 10^{12}$ N/m.

### 4.3. Constraints on the Formation and Evolution of the Iberian-European Plate Boundary Fault

If intraplate deformation in Central Europe was caused by plate boundary compression, then the force required to drive intraplate deformation provides a gauge for the magnitude of $F_S$ that must have been provided to allow deformation in the interior of the continent. Numerical simulations of basin inversion in Central Europe indicate that the force required to drive deformation was at the order of ~3–4 $\times 10^{12}$ N/m, where the exact value depends on the thermal and rheological properties of the lithosphere (e.g., Nielsen

et al., 2007; Nielsen & Hansen, 2000; Sandiford, 1999). For simplicity, we assume that intraplate deformation is plausible if $F_S \geq 3 \times 10^{12}$ N/m and implausible if $F_S < 3 \times 10^{12}$ N/m. We note that the question of whether a given magnitude of $F_S$ suffices to drive intraplate deformation depends also on how the force is distributed across the lithosphere and the resultant magnitude of the horizontal deviatoric stress transmitted into the plate. The inversion of rift basins such as in Central Europe is favored by strong deviatoric compression at crustal levels, that is, within the upper ~30 km of the lithosphere (e.g., Burov & Diament, 1995). We therefore calculated for both settings the average differential stress that is induced in the upper 30 km (Figures 7e and 7f). These calculations serve mainly to illustrate how the horizontal deviatoric compression varies with the rheology of the fault. We note, however, that the calculated stresses provide only a rough estimate for the actual stress magnitude in Central Europe, because there was likely some stress dissipation laterally to the east and west as well as along structural and rheological discontinuities that we cannot account for here. The transfer of stresses into the far field has been simulated by Nielsen et al. (2007) by means of numerical spherical stress models and is beyond the aim of this work.

The above constraints on the force required to drive intraplate deformation allow to assess the basic evolution of the IEPB fault during Late Cretaceous to early Paleocene time. Our findings suggest that at the onset of plate convergence the strength of the lithosphere beneath the hyperextended rift was only slightly higher than the force required to drive intraplate deformation (dashed line in Figure 7c). If there was a fault that was weakened to a depth greater than ~10 km, then $F_S$ would become too small to allow intraplate deformation in Central Europe. This suggests that there was either no lithospheric-scale fault at the onset of plate convergence, in which case the force driving plate convergence was directly transferred into Europe, or that there was a lithospheric-scale fault whose strength was similar to that of the lithosphere. Perhaps, the most consistent interpretation is that the driving force was initially transferred into Europe but overcame the yield strength of the lithosphere resulting in the formation of a new convergent plate boundary fault. In this case, deformation should have been initially distributed across the rift system but progressively localized into a discrete fault system. We suppose that with the localization the fault started to weaken rheologically.

Around the early Paleocene, $F_S$ must have decreased to a magnitude below $3 \times 10^{12}$ N/m to end the strong horizontal deviatoric compression of Europe. We find that the required decrease in $F_S$ is compatible with a weakening of the fault within the upper ~30–35 km. This suggests that the IEPB fault was localized and weakened around the end of the Late Cretaceous. In contrast, if the fault were not or only slightly weakened, the plate coupling force would have increased significantly resulting in an even stronger compression of Europe.

### 4.4. Numerical Simulation of Hyperextended Rift Inversion

The calculation of the plate coupling force is based on presumptions and simplifications that were made in accordance with geological data and reconstructions; however, key parameters are not directly accessible. This relates in particular to the lithosphere thickness and thermal gradient after hyperextension as well as the localization of the fault within the exhumed mantle domain. Moreover, we treat the IEPB fault for both settings as a coherent planar structure, which may be inappropriate, especially for the earliest evolution of the fault. Likewise, the calculations do not account for deformation in the surrounding lithosphere.

To evaluate the robustness of our findings, we performed numerical simulations of the inversion of a hyperextended rift system using the thermomechanical finite element model SLIM3D (Popov & Sobolev, 2008), which has been previously applied in elucidating structures and dynamics of continental rift systems (Brune et al., 2014, 2016; Brune, Corti, et al., 2017; Brune, Heine, et al., 2017). Parameters are identical to those of the West Iberian rift model in Brune et al. (2014) with an initial (prerifting) thermal LAB (1300 °C isotherm) at 105-km depth. In contrast to the previous model, we here reproduce first-order kinematics of the Pyrenean region by continuing the simulation with a brief phase of tectonic quiescence that is followed by long-term shortening. A sketch of the initial setup is given in Figure 8a. During the rift phase, the model is extended at a rate of 4 mm/year at the lateral boundaries, resulting in a net extension rate of 8 mm/year. Extension stops after 20 Myr. At this stage, a narrow asymmetric hyperextended rift system has formed with mantle exhumation and limited crustal breakup in the rift center (Figure 8b). After extension, the model remains at rest for 5 Myr to account for postrift thermal relaxation. Subsequently, the model is shortened at a rate of 2 mm/year at the lateral boundaries (4 mm/year net shortening rate).

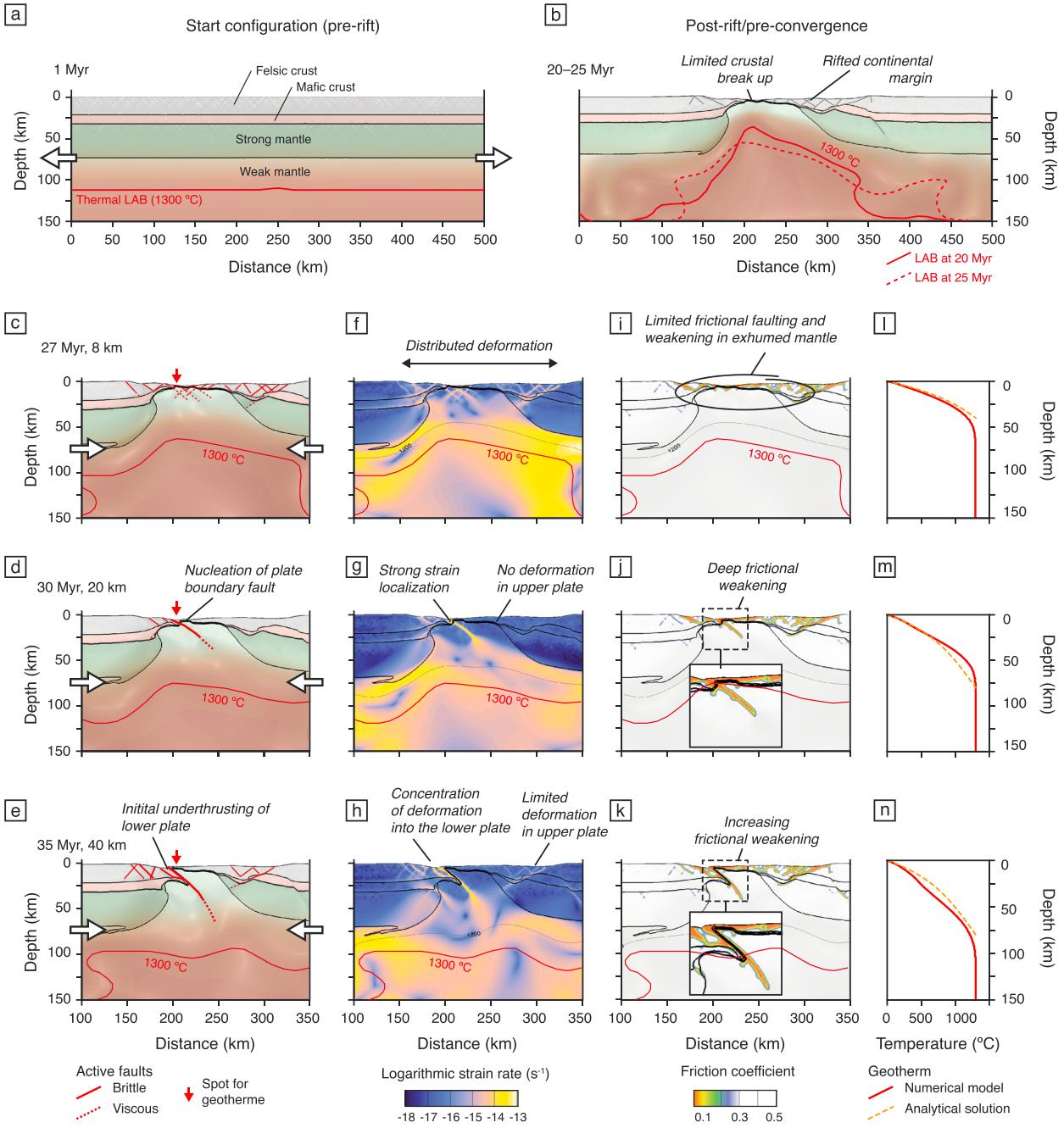


**Figure 8.** Setup and key variables of the numerical simulations of hyperextension followed by convergence and inversion, showing in particular the initiation of the plate boundary fault. (a) Model setup. LAB = lithosphere-asthenosphere boundary. (b) Postrift/preconvergence margin structure. (c–e) Fault kinematics. (f–h) Strain rate. (i–k) Friction coefficient. (l–n) Geotherms derived from the numerical simulations. Localities of the vertical depth profiles are indicated by the red arrows in Figures 8c–8e. Orange dashed line shows the geotherms derived from analytical solutions for comparison.

With the onset of shortening the rift domain experiences a phase of distributed deformation along both margins and within the exhumed mantle domain (Figures 8c and 8f). Along the margins, frictional faulting dominates and reactivates rift-inherited structures (Figure 8i). In the exhumed mantle domain, new conjugate faults and viscous shear zones form within the upper ~30 km (Figure 8f). Frictional faulting is restricted to the uppermost kilometers. After ~20 km of shortening, deformation is localized into a single fault that cuts through the mantle domain and represents the principal plate boundary fault (Figures 8d and 8g). The fault deforms frictionally in the upper ~25 km and as a viscous shear zone below. Simultaneously, deformation in

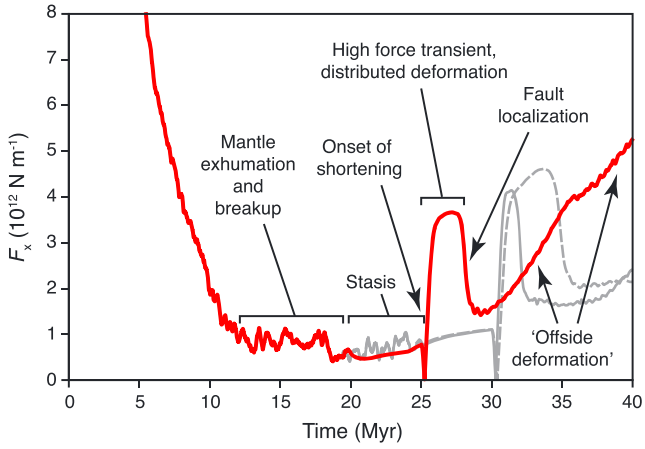


**Figure 9.** Temporal evolution of the horizontal force $F_X$ applied to extend or shorten the model at a given rate. Red line is for the reference model (20-Myr rifting followed by shortening at a rate of 4 mm/year), gray solid line for alternative model 1 (25-Myr rifting, 4 mm/year shortening), and gray dashed line for alternative model 2 (25-Myr rifting, 2 mm/year shortening).

the upper plate (hanging wall of the main fault) stops, while restricted frictional faulting occurs in the lower plate (Figures 8g and 8j). In the following evolution stage, the plate boundary fault continues to weaken and the frictional segment extends to greater depth (Figures 8e, 8h, and 8k). Deformation is largely accommodated along the plate boundary fault and along new faults that form in the lower plate, while limited frictional faulting occurs in the upper plate along existing structures. This evolution agrees with recently published numerical results addressing the role of rift maturity on the shortening distribution in the Pyrenees (Jourdon et al., 2019). Throughout the evolution of our model, the LAB beneath the rift center descends from ~50 km depth at the onset of shortening to ~90-km depth after 40 km of shortening (Figures 8l–8n).

To further examine the localization and weakening of the plate boundary fault, we calculated the horizontal force $F_X$, which is the force required to extend or shorten the model at a given rate. The force $F_X$ is computed through vertical integration of the tectonic stress and reflects the bulk deformation of the entire model lithosphere (Brune et al., 2012, 2013). The force $F_X$ is therefore not always comparable to the plate coupling force $F_S$, which describes the strength of the plate boundary fault only.

Figure 9 shows the evolution of $F_X$ as a function of time. At the end of rifting, $F_X$ drops below ~$1 \times 10^{12}$ N/m and remains at a low value throughout the subsequent postrift phase, during which the model lithosphere experiences only limited deformation due to the thermal relaxation. With the onset of shortening, $F_X$ rises quickly to ~$3.5 \times 10^{12}$ N/m and remains at this level as long as deformation is distributed across the rift system, where the magnitude of $F_X$ is primarily controlled by deformation within the upper mantle (Figure 8c). As the plate boundary fault localizes, $F_X$ drops to ~$1.5 \times 10^{12}$ N/m. At this stage, deformation is concentrated along the plate boundary fault and $F_X$ provides an approximate measure for its strength (Figure 8d). After the localization and weakening of the fault, $F_X$ increases gradually to values >4–5 $\times 10^{12}$ N/m ("offside deformation" in Figure 9). Interestingly, this increase in $F_X$ is not related to deformation along the plate boundary fault that remains weak (Figure 8e), but mirrors enhanced deformation in the model lithosphere offside the rift system, especially around the Moho of the lower plate. With respect to the development in the Pyrenean realm, this suggests that Iberia experienced strong compression during underthrusting. We suggest that this is reflected by the ~NE-SW directed, Eocene to Miocene inversion of Mesozoic basins in the Iberian chain, south of the Pyrenees (section 3; Figure 3; Guimerà et al., 2004). Notably, in the numerical simulations such an inversion does not occur, because the model lithosphere is not structurally weakened offside the rift system.

In summary, the numerical simulation corroborates the assumptions made for the analysis of the plate coupling force. In particular, the depth of the LAB and the resultant thermal gradients beneath the rift center (Figures 8l–8n) vary only slightly from the one used for the calculation of $F_S$ (Figure 7). The numerical simulation also indicates a formation of the plate boundary fault in the exhumed mantle domain, consistent with our assumptions above and previous geological reconstructions (section 2.2). Moreover, the plate boundary fault develops as a new structure that progressively spreads in depth and weakens with ongoing convergence (cf. Jourdon et al., 2019), which supports our interpretation of the formation and evolution of the IEBP fault based on the analysis of $F_S$.

In the numerical models, the high force transient related to the nucleation of the plate boundary fault lasts for the first ~3–4 Myr of shortening. In contrast, the geological constraints from the Pyrenean realm and Central Europe indicate that the high force transient lasted longer, about 15–20 Myr, which suggests that the localization and weakening of the IEPB fault was slower in nature. To test whether the difference in the timing relates to the shortening rate or to the magnitude of extension prior to shortening, we performed two additional model runs. The first model run is identical to the reference model, but the rifting continues for another 5 Myr, which translates to an additional 40 km of extension (gray solid line in Figure 9). The second model run is identical to the latter, but the full shortening rate is reduced by 50% to 2 mm/year (gray dashed line in Figure 9). Overall, the alternative models show an evolution comparable to that of the

reference model. Differences exist in the magnitude of $F_X$ and the time required to localize the plate boundary fault (~2–3 and ~5–6 Myr for alternative models 1 and 2, respectively; Figure 9). However, the differences are too small to explain the inferred disparity between the duration of fault localization in nature and model. Interestingly, a similar picture emerges from geological and numerical constraints on induced subduction initiation, that is, the formation of a convergent plate boundary fault and development of a self-sustained subduction zone in response to convergence (e.g., Stern, 2004). Numerical simulations predict a high force transient within the upper plate for the first ~2–3 Myr of convergence related to the formation of the plate boundary fault (Gurnis et al., 2004). For comparison, geological data from the Tonga-Kermadec subduction zone suggest that the Eocene subduction initiation was associated with ~10- to 20-Myr-long pulse of widespread deviatoric compression in the upper plate driving deformation in the near field and far field of the fault (Sutherland et al., 2017). This suggests that the localization and weakening of the plate boundary fault lasted longer than suggested by numerical simulations, similar to our findings. However, whether the durations inferred for the formation of the IEPB fault and the Tonga-Kermadec subduction megathrust are representative for the time needed to form a new plate boundary fault is yet to be understood.

## 5. Discussion

Our results indicate that the strength of the lithosphere beneath the hyperextended rift system was about 3.5 $\times 10^{12}$ N/m at the onset of plate convergence. Compared to normal continental lithosphere with a strength of more than $10^{13}$ N/m, the lithosphere was substantially weakened. The numerical simulations show that the low strength was mainly thermally controlled and related to the shallow LAB resulting from rifting and hyperextension and associated mantle upwelling. At the same time, the strength of the lithosphere was just high enough to allow an upper plate compression sufficient to drive intraplate deformation. Notably, these conditions were directly facilitated by the presence of mantle rocks at or close to the surface. Our findings further suggest that the lithosphere beneath the Pyrenean realm rethickened and cooled throughout the Late Cretaceous, which successively increased its strength. Simultaneously, the IEPB fault progressively localized and weakened. This development of the fault competed probably with the restrengthening of the lithosphere, which allowed maintaining the strong compression of Europe during Late Cretaceous time. At the transition to the Paleocene the fault was weakened within the upper ~30–40 km, thus eventually terminating strong compression of Europe and ending intraplate deformation.

### 5.1. Role of Serpentinization and Rift-Inheritance for the Formation of the Iberian-European Plate Boundary Fault

Our results suggest that the IEPB fault formed as a new structure and that the formation of the fault in the mantle domain was to a first-order controlled by thermal weakening of the lithosphere due to previous hyperextension. This finding is consistent with previous studies that also envisaged a strong thermal control on the initial accommodation of plate convergence within the mantle domain (e.g., Tugend et al., 2015). Another factor that is commonly assumed to have controlled the localization of the plate boundary fault is the partial serpentinization of mantle rocks close to Earth's surface, which reduces the strength of mantle rocks considerably (Chevrot et al., 2018; Escartín et al., 2001; Roca et al., 2011; Tugend et al., 2014, 2015). For the evaluation of the plate coupling force, we account for a serpentinization within the upper 5 km of the mantle lithosphere (Figure 6a). If we replace for Setting I, the serpentinites by normal mantle lithosphere, then the strength of the lithosphere increases by ~24% from $3.4 \times 10^{12}$ to $4.2 \times 10^{12}$ N/m (supporting information Figure S1), which shows that serpentinization has a relevant impact on the strength of the lithosphere beneath the rift center. To further evaluate the importance of serpentinization, we estimated also the strength of the rifted continental margin, based on the numerical simulations presented herein. Depending on the thermal state, the strength of the rifted margin is between ~$6 \times 10^{12}$ and ~$11 \times 10^{12}$ N/m (supporting information Figure S2). These strength estimates are significantly higher than the inferred strength of the lithosphere in the exhumed mantle domain, irrespective of whether the mantle is serpentinized or not. This suggests that in either case the plate boundary fault should localize in the exhumed mantle domain, as it is the weakest domain in the entire rift system shortly after hyperextension. We therefore suggest that serpentinization was probably relevant for strain localization in the upper kilometers but did not condition the formation of the IEPB fault in the mantle domain.

Alternatively, it was proposed that plate convergence was accommodated by the reactivation of a rift-inherited extensional detachment fault flanking the exhumed mantle domain (e.g., Jammes et al., 2009). At present, there is no indication for the existence of such a fault and it is not clear to which depths this fault potentially extended or what the rheology of this fault was. Our evaluation of the plate coupling force indicates that the reactivation of a weak rift-inherited fault at depths >10 km is inconsistent with the strong compression of Europe. Besides, the numerical models presented herein and in greater detail in Brune et al. (2014) indicate that weak brittle faults form during hyperextension only in the stretched continental crust and in the uppermost part of the exhuming mantle, but not at greater depths where the temperature in the mantle is so high that the mantle deforms in a viscous manner. A reactivation of inherited ductile shear zones may be problematic, because viscous strain softening is linked to deformation mechanisms, which depend on the temperature and stress conditions during deformation (e.g., de Bresser et al., 2001). During exhumation and cooling of rocks the deformation conditions change and inherited ductile shear fabrics may not remain weak in the changing environment. Moreover, weak shear fabrics may be annealed during quasi-static recrystallization processes, which would also help to recover the strength of the lithosphere (e.g., Matysiak & Trepmann, 2015; Trepmann et al., 2013). We therefore propose that the lithospheric-scale reactivation of a rift-inherited extensional detachment fault is unlikely and was probably restricted to the upper ~5–10 km.

### 5.2. Differences in the Tectonic Setting Along-Strike the Iberian-European Plate Boundary

Our study focuses on the development of the IEBP fault in the Pyrenees that has a present east-west extent of about 400 km (Figure 3). However, the present-day extent of the Pyrenees represent only a part of the original IEPB that reached from the Bay of Biscay area to Provence (southeast France) where it probably continued into the Alpine realm (Figure 1b; Lacombe & Jolivet, 2005; Macchiavelli et al., 2017; Roca et al., 2011; Schettino & Turco, 2011; Séranne, 1999; Stampfli et al., 1998; Tugend et al., 2015). Notably, shortening in response to Africa-Iberia-Europe convergence is documented all along the North Iberian Margin in the west to Provence in the east, which suggests an original east-west extent of the convergent plate boundary fault of ~1,000–1,200 km (Leleu et al., 2009; Roca et al., 2011; Tugend et al., 2014). We therefore anticipate that the transfer of tectonic forces into Europe was not restricted to the present-day Pyrenean realm. For comparison, the east-west extent of the Late Cretaceous inversion zones in Central Europe is also about 1,000–1,200 km, which suggests that the transfer of tectonic forces occurred over much of the original extent of the convergent plate boundary. This implies that our principal finding that the compression of Europe was governed by the evolving strength of the convergent plate boundary fault should also apply to other segments of the plate boundary. In the following, we address some major differences in the tectonics to the west and to the east of the Pyrenees.

#### 5.2.1. Bay of Biscay-Cantabrian Mountains

The western continuation of the Pyrenees is represented by the Cantabrian Mountains that strike along the North Iberian Margin until ~6°–7°W (Figure 3). The North Iberian Margin transitions northward into the Bay of Biscay, a narrow V-shaped oceanic basin that developed as a failed arm of the Atlantic between Iberia and Europe throughout the Mesozoic. Compared to the Pyrenean domain, hyperextension and mantle exhumation occurred earlier in the Bay of Biscay and were followed by seafloor spreading, though the spatial and temporal evolution of hyperextension and seafloor spreading varies throughout the Bay of Biscay (Pedreira et al., 2015; Sibuet et al., 2004; Tugend et al., 2014, 2015). In the eastern part of the Bay of Biscay there was no seafloor spreading, but rifting resulted in the formation of two subbasins; the Basque-Cantabrian Basin in the south and the Parentis Basin in the north that are separated by a block of European continental crust, the Landes High (Figure 3). Geological reconstructions of the two basins indicate that rifting lasted in the Parentis Basin from around 130–106 Ma (Barremian to Albian), while it continued in the Basque-Cantabrian Basin, where it culminated in hyperextension and the exhumation of subcontinental mantle lithosphere to the surface, analogous to the Pyrenean domain (Tugend et al., 2014, 2015). In the central part of the Bay of Biscay, magnetic anomalies (M3, M0) suggest that rifting was followed by seafloor spreading between 124 to 118 Ma (Aptian), but there are no constraints on the continuation of seafloor spreading after the Aptian (Figure 3; Sibuet et al., 2004). Only in the western Bay of Biscay (west of 8°W) are magnetic anomalies documented (A34) that indicate seafloor spreading until ~84–80 Ma (Sibuet et al., 2004; Sibuet & Collette, 1991).

Plate kinematic reconstructions indicate that convergence between Iberia and Europe in the Bay of Biscay area started in the Late Cretaceous around 84 Ma (i.e., similar to the Pyrenean domain) except for the area west of ~7°–8°W, where plate convergence is reported to have started later around the Paleocene-Eocene boundary (Macchiavelli et al., 2017). East of approximately 7°W, plate convergence was accommodated by underthrusting Iberia beneath the North Iberian Margin, which was associated with the inversion of the Basque-Cantabrian Basin and the uplift of the Cantabrian Mountains (Diaz et al., 2016; Pedreira et al., 2003, 2007; Roca et al., 2011; Ruiz et al., 2017). At the same time, the North Iberian Margin experienced shortening, which is documented by thrust faulting and reactivation of rift-inherited faults preferentially within the distal parts of the margin (Alvarez-Marron et al., 1997; Cadenas & Fernández-Viejo, 2016; Fernández-Viejo et al., 2012; Gallastegui et al., 2002; Tugend et al., 2014). The shortening along the North Iberian Margin has been interpreted to record limited southward subduction of the Bay of Biscay lithosphere beneath the North Iberian Margin, although this hypothesis remains poorly constrained and disputed (Alvarez-Marron et al., 1997; Fernández-Viejo et al., 2012; Gallastegui et al., 2002; Pedreira et al., 2015; Roca et al., 2011; Teixell et al., 2018). Both the underthrusting of Iberia and the potential limited subduction of the Bay of Biscay are thought to have started during the Early Eocene (e.g., Fernández-Viejo et al., 2012; Pedreira et al., 2015). This timing is, however, poorly constrained, and it remains difficult to understand why the underthrusting of Iberia and the possible subduction of the Bay of Biscay should have started in the Eocene and not directly at the Late Cretaceous onset of plate convergence.

The complexity in the extensional history of the Bay of Biscay and the uncertainties in the timing and distribution of shortening in response to plate convergence make it problematic to directly transfer our findings from the Pyrenean realm to the Bay of Biscay area without additional data. Independently, the underthrusting of Iberia beneath the North Iberian Margin can be traced until ~6°–7°W and appears in continuity with the underthrusting of Iberia beneath the Pyrenees (Figure 3; Pedreira et al., 2007, 2015; Roca et al., 2011; Teixell et al., 2018). We therefore suggest that the fault system that allowed the underthrusting of Iberia beneath the North Iberian Margin represents the westward continuation of IEPB fault. We further suppose that the development of this fault started already during the Late Cretaceous as in the Pyrenean domain. Notably, this does not contradict that the main phase of underthrusting commenced during the Eocene. To the contrary, this development would be similar to the evolution in the Pyrenean domain, where the main phase of underthrusting also occurred during the Eocene. If our interpretations are correct, the Late Cretaceous development of the IEPB fault was probably restricted to ~6°–7°W, which would be consistent with plate kinematic reconstructions indicating that plate convergence further west started after the Late Cretaceous (e.g., Macchiavelli et al., 2017).

#### 5.2.2. Eastern Pyrenees-Provence

The present-day structure of the lithosphere beneath the Pyrenees exhibits a pronounced change from the central to the eastern Pyrenees that is geophysically well constrained by seismic reflection and receiver function studies (Chevrot et al., 2018; Diaz et al., 2018; Gallart et al., 2001). First, the depth of the crust-mantle boundary (Moho) beneath the Pyrenees decreases from west to east over a distance of ~130–150 km from about ~45- to ~20-km depth near the coastline of the Mediterranean Sea. Moreover, the slab of the Iberian plate that is well imaged beneath the western and central Pyrenees is not imaged on profiles across the eastern Pyrenees, east of ~1.3°E. Instead, the imaged Moho beneath eastern Pyrenees is slightly segmented and varies between ~40 and ~35 km beneath the orogen (Diaz et al., 2018). Both the thinning of the crust and the missing slab beneath the eastern Pyrenees have been interpreted to document a thermal and/or mechanical erosion of the lithosphere related to Oligocene to Miocene extension caused by the rollback of the Tyrrhenian slab (e.g., Gallart et al., 2001; Gunnell et al., 2008; Séranne, 1999).

It has also been suggested that the present-day Moho beneath the eastern Pyrenees preserves, in part, the original crustal structure at the end of the Pyrenean orogeny, in particular in the absence of the Iberian slab, implying that there never was an Iberian slab in the east (Chevrot et al., 2018; Diaz et al., 2018). This interpretation considers recent reconstructions of the postrift architecture of the eastern Pyrenees, which suggest that hyperextension resulted in the formation of two major subbasins that were separated by small continental blocks, now preserved as the North Pyrenean massifs (Clerc et al., 2015, 2016). In detail, these reconstructions indicate a larger southern subbasin that was floored by exhumed mantle rocks and a northern subbasin that overlay strongly thinned continental crust. In this light, it has been hypothesized that this segmented rift structure in the eastern Pyrenees conditioned a more broadly distributed

deformation during the orogeny and that plate convergence was accommodated by the closure of the rift basins (Chevrot et al., 2018; Diaz et al., 2018). Moreover, it has been suggested that plate convergence stopped after the subbasins were closed and Iberia and Europe collided with the continental blocks between them, which could explain the present-day segmented structure of the Moho in the eastern Pyrenees (Diaz et al., 2018).

If the above interpretations are correct, then the closure of the two subbasins was accommodated by the creation of two major fault systems. The geometry of the segmented Moho and the presence of north dipping seismic velocity anomalies in the overlying crust (Chevrot et al., 2018) that may represent crustal shear zones are coherent with this conjecture. In this case, our analysis of the plate coupling force and early development of the IEPB would be most appropriate for the fault system that facilitated the closure of the larger southern subbasin, which was floored by exhumed mantle rocks. Because plate convergence was distributed more broadly, this new plate boundary fault did probably not evolve to accommodate subduction of Iberian crust into the mantle during Eocene to Miocene time. It is important to note that a segmentation of the IEPB may influence the stress state in the near field but would not affect the general development of plate coupling considered here.

The continuation of the IEPB east of the Pyrenees was largely obliterated by the Alpine orogeny and the Oligocene to Miocene opening of the Gulf of Lion and therefore remains speculative. Nevertheless, the Provence fold and thrust belt is generally accepted to represent the northeastern continuation of the northern Pyrenees (Séranne, 1999; Stampfli et al., 1998). This fold and thrust belt records Triassic to Cretaceous extension, followed by Late Cretaceous to Eocene N-S directed shortening (Bestani et al., 2016; Leleu et al., 2009; Mauffret & Gorini, 1996). Recently, up to 2,000 m of Apto-Albian strata have been reported offshore Marseille by Fournier et al. (2016), suggesting that Apto-Albian major rift system continued east from the Pyrenees (see also Tavani et al., 2018). Whether the rifting resulted in the exhumation of mantle rocks and limited crustal break up as in the Pyrenees is not clear. However, we may suppose that the Late Cretaceous to Eocene tectonics of the Provence area requires an eastern continuation of the IEPB fault and that the earliest evolution of the fault was comparable to the one further west.

### 5.3. Effects of Plate Coupling on the Early Tectonics in the Pyrenees

Our study establishes a linkage between formation and rheological evolution of the IEPB fault and deformation in the far field, that is, in Central Europe. The development of the fault must have also governed the deformation in the near field of the plate boundary. In the following we summarize some major aspects of the earliest tectonics in the Pyrenees that we interpret to trace the rheological evolution of the IEPB fault.

The inversion of the rifted continental margins of Iberia and Europe indicate an immediate response to the onset of Late Cretaceous plate convergence. The inversion took place before the actual margins collided and was accompanied by the northward thrusting of the metamorphic sediments that originally covered the exhumed mantle domain (section 2.2). In the central to eastern Pyrenees, the Late Cretaceous inversion of the European margin accounts for ≥50% of the shortening (~11 km) that was accommodated in the Northern Pyrenees until the end of the orogeny (~20 km; e.g., Grool et al., 2018). Likewise, the North Pyrenean Foreland Basin accommodated ~50% of its total subsidence already during the Late Cretaceous (first subsidence phase in Figure 2a; Ford et al., 2016; Grool et al., 2018; Rougier et al., 2016). At this stage, there was not yet a well-developed orogenic wedge that could explain the strong tectonic subsidence as an isostatic response to gravitational loading of the European lithosphere. The distinct acceleration of subsidence around 84 Ma is difficult to reconcile solely with a continuous postrift thermal relaxation of the lithosphere (Angrand et al., 2018) and was probably controlled by the initial inversion of continental basement blocks along rift inherited normal faults. The distributed deformation and the precollisional inversion of the European margin and associated development of the NPFB document widespread horizontal compression in the Pyrenean realm, which is consistent with an efficient transfer of tectonic forces from Iberia into Europe during the Late Cretaceous.

Around the Paleocene, the mantle domain between Iberia and Europe was closed and the distal Iberian margin started to underthrust Europe, which suggests that the IEPB fault formed a discrete, localized structure. Around the same time, subsidence in the NPFB was interrupted by a ~7-Myr-long period that lasted until the

late Paleocene (second subsidence phase in Figure 2a). This quiet period was characterized by the accumulation of a thin (~100 m), condensed succession and a stagnation of the basin margin. The sedimentary facies document a reduced clastic input, a low stream energy, and a low relief in the hinterland, indicating that the inversion of the southern European margin ceased (Ford et al., 2016). This halt of margin inversion is consistent with a weak plate coupling and upper plate compression by the end of the Late Cretaceous. Interestingly, a similar dynamic occurs in the numerical simulations, where deformation is initially distributed across the entire rift system but ceases in the upper plate as the major fault localizes and spreads in depth.

After the Paleocene the tectonics in the Pyrenees changed. Iberia and Europe collided and most of the plate convergence was accommodated in the Southern Pyrenees, as recorded by the successive accretion of the Iberian basement units and the propagation of the southern foreland fold and thrust (section 2.2). In contrast, the Northern Pyrenees experienced only limited additional shortening by open to tight folding and slip on existing faults, but there is no remarkable propagation of new thrust faults into the foreland, except for the Sub-Pyrenean Thrust (Figure 4c; e.g., Deramond et al., 1993; Ford et al., 2016). Moreover, deformation was mainly generated by backthrusting of the growing pro-wedge rather than to continuous margin inversion and subsidence in the NPFB became controlled by the gravitational loading of the European lithosphere (third subsidence phase in Figure 2a; Ford et al., 2016; Grool et al., 2018; Sinclair, 2005). These findings are consistent with a continued low coupling along the IEPB fault and a restricted transfer of tectonic forces into Europe.

## 6. Summary and Conclusions

We integrated mechanical considerations, numerical simulations, and geological reconstructions of the Pyrenean realm to evaluate how the Late Cretaceous formation of the convergent Iberian-European plate boundary fault affected intraplate deformation in Central Europe. We propose that the fault developed as a new structure in the hyperextended rift system separating Iberia and Europe at the onset of plate convergence. The initial strength of the lithosphere beneath the rift system allowed a strong coupling of Iberia and Europe and an efficient transmission of compressive stresses far into Europe. Consequently, Central Europe experienced area-wide deviatoric compression, which was strong enough to drive intraplate shortening within areas of reduced crustal strength. At the end of the Cretaceous, the Iberian-European plate boundary fault was localized into a discrete lithospheric-scale structure that weakened rheologically. Consequently, the coupling between Iberia and Europe declined and the deviatoric compression as well as the deformation in the interior of Europe ceased. The termination of deformation may have been accentuated by a slowdown or potential interruption in north directed Africa-Iberia-Europe convergence during the Paleocene, but further research is required to better constrain the nature of this event. Independently, when plate convergence accelerated (or restarted) the coupling between Iberia and Europe remained weak and there was no other phase of intense deviatoric compression in Central Europe triggered by the Pyrenean orogeny or Africa-Iberia-Europe convergence. In contrast, large parts of Europe experienced deviatoric tension as recorded by the opening of Cenozoic rift systems. Notably, the formation and evolution of the Iberian-European plate boundary fault exerted also a strong control on the tectonics in the near field, that is, in the Pyrenean realm. This relates in particular to the initially broad distribution of deformation, affecting both the upper and the lower plate, and the subsequent concentration of deformation into the lower plate as soon as the Iberian-European plate boundary fault was localized and weakened.

On a general note, we find that intraplate deformation occurred in response to a major change in the plate tectonic framework, that is, due to the onset of plate convergence and the formation of a plate boundary fault. Similarly, previous studies concluded that intraplate deformation occurred during a rearrangement of the geodynamic setting (Bosworth et al., 1999; Sutherland et al., 2017). This encourages to view intraplate deformation events as a record of high force (or stress) transients that occur in response to changes in the plate tectonic framework, rather than understanding them as general response to convergence and collision. In this sense, the deformation record of continental interiors may provide a suitable proxy to reconstruct how the lithosphere reacted to certain disturbances and how its strength evolved in time.

**Acknowledgments**

This study is part of the Orogen research program and was funded by Total (France), the BRGM (Bureau de Recherches Géologiques et Minières, France), and the CNRS (Centre National de la Recherche Scientifique, France), which is greatly acknowledged. S. B. was funded through the Helmholtz Young Investigators Group CRYSTALS (VH-NG-1132). We would like to thank Jonas Kley and two anonymous reviewers for providing detailed and thoughtful comments, which helped us to clarify a number of issues and to improve the readability of the manuscript. We thank Onno Oncken, Marcos Moreno, and Emmanuel Masini for critical comments and discussion. All data used in this study are from the published literature as cited in the text. Details on the calculation of the plate coupling force are given in the supporting information. The authors declare no competing financial interests.

## References

Alvarez-Marron, J., Rubio, E., & Torne, M. (1997). Subduction-related structures in the North Iberian Margin. *Journal of Geophysical Research*, *102*(B10), 22,497–22,511. https://doi.org/10.1029/97JB01425

Angrand, P., Ford, M., & Watts, A. B. (2018). Lateral variations in foreland flexure of a rifted continental margin: The aquitaine basin (SW France). *Tectonics*, *37*, 430–449. https://doi.org/10.1002/2017TC004670

Ardévol, L., Klimowitz, J., Malagón, J., & Nagtegaal, P. J. C. (2000). Depositional sequence response to foreland deformation in the upper Cretaceous of the Southern Pyrenees, Spain. *AAPG Bulletin*, *84*(4), 566–588. https://doi.org/10.1306/C9EBCE55-1735-11D7-8645000102C1865D

Bachmann, R., Glodny, J., Oncken, O., & Seifert, W. (2009). Abandonment of the South Penninic-Austroalpine palaeosubduction zone, Central Alps, and shift from subduction erosion to accretion: constraints from Rb/Sr geochronology. *Journal of the Geological Society*, *166*(2), 217–231. https://doi.org/10.1144/0016-76492008-024

Beaumont, C., Muñoz, J. A., Hamilton, J., & Fullsack, P. (2000). Factors controlling the Alpine evolution of the central Pyrenees inferred from a comparison of observations and geodynamical models. *Journal of Geophysical Research*, *105*(B4), 8121–8145. https://doi.org/10.1029/1999JB900390

Bestani, L., Espurt, N., Lamarche, J., Bellier, O., & Hollender, F. (2016). Reconstruction of the Provence Chain evolution, southeastern France. *Tectonics*, *35*, 1506–1525. https://doi.org/10.1002/2016TC004115

Bosworth, W., Guiraud, R., & Kessler, L. G. (1999). Late Cretaceous (ca. 84 Ma) compressive deformation of the stable platform of northeast Africa (Egypt): Far-field stress effects of the "Santonian event" and origin of the Syrian arc deformation belt. *Geology*, *27*(7), 633–636. https://doi.org/10.1130/0091-7613(1999)027<0633:LCCMCD>2.3.CO;2

Bourgeois, O., Ford, M., Diraison, M., Veslud, C. L. C. ., Gerbault, M., Pik, R., et al. (2007). Separation of rifting and lithospheric folding signatures in the NW-Alpine foreland. *International Journal of Earth Sciences*, *96*(6), 1003–1031. https://doi.org/10.1007/s00531-007-0202-2

Brune, S., Corti, G., & Ranalli, G. (2017). Controls of inherited lithospheric heterogeneity on rift linkage: Numerical and analog models of interaction between the Kenyan and Ethiopian rifts across the Turkana depression. *Tectonics*, *36*, 1767–1786. https://doi.org/10.1002/2017TC004739

Brune, S., Heine, C., Clift, P. D., & Pérez-Gussinyé, M. (2017). Rifted margin architecture and crustal rheology: Reviewing Iberia-Newfoundland, Central South Atlantic, and South China Sea. *Marine and Petroleum Geology*, *79*, 257–281. https://doi.org/10.1016/J.MARPETGEO.2016.10.018

Brune, S., Heine, C., Pérez-Gussinyé, M., & Sobolev, S. V. (2014). Rift migration explains continental margin asymmetry and crustal hyper-extension. *Nature Communications*, *5*(1), 4014. https://doi.org/10.1038/ncomms5014

Brune, S., Popov, A. A., & Sobolev, S. V. (2012). Modeling suggests that oblique extension facilitates rifting and continental break-up. *Journal of Geophysical Research*, *117*, B08402. https://doi.org/10.1029/2011JB008860

Brune, S., Popov, A. A., & Sobolev, S. V. (2013). Quantifying the thermo-mechanical impact of plume arrival on continental break-up. *Tectonophysics*, *604*, 51–59. https://doi.org/10.1016/j.tecto.2013.02.009

Brune, S., Williams, S. E., Butterworth, N. P., & Müller, R. D. (2016). Abrupt plate accelerations shape rifted continental margins. *Nature*, *536*(7615), 201–204. https://doi.org/10.1038/nature18319

Burov, E. B., & Diament, M. (1995). The effective elastic thickness (T e) of continental lithosphere: What does it really mean? *Journal of Geophysical Research*, *100*(B3), 3905–3927. https://doi.org/10.1029/94JB02770

Cadenas, P., & Fernández-Viejo, G. (2016). The Asturian Basin within the North Iberian margin (Bay of Biscay): Seismic characterisation of its geometry and its Mesozoic and Cenozoic cover. *Basin Research*, *29*(4), 521–541. https://doi.org/10.1111/bre.12187

Chevrot, S., Sylvander, M., Diaz, J., Martin, R., Mouthereau, F., Manatschal, G., et al. (2018). The non-cylindrical crustal architecture of the Pyrenees. *Scientific Reports*, *8*(1), 9591. https://doi.org/10.1038/s41598-018-27889-x

Chevrot, S., Sylvander, M., Diaz, J., Ruiz, M., & Paul, A. (2015). The Pyrenean architecture as revealed by teleseismic P-to-S converted waves recorded along two dense transects. *Geophysical Journal International*, *200*(2), 1094–1105. https://doi.org/10.1093/gji/ggu400

Choukroune, P., & ECORS-Pyrenees-Team (1989). The Ecors Pyrenean deep seismic profile reflection data and the overall structure of an orogenic belt. *Tectonics*, *8*(1), 23–39. https://doi.org/10.1029/TC008i001p00023

Choukroune, P., & Mattauer, M. (1978). Tectonique des plaques et Pyrenees; sur le fonctionnement de la faille transformante nord-pyreneenne; comparaisons avec des modeles actuels. *Bulletin de La Société Géologique de France*, *7*(5), 689–700.

Clerc, C., & Lagabrielle, Y. (2014). Thermal control on the modes of crustal thinning leading to mantle exhumation: Insights from the Cretaceous Pyrenean hot paleomargins. *Tectonics*, *33*, 1340–1359. https://doi.org/10.1002/2013TC003471

Clerc, C., Lagabrielle, Y., Labaume, P., Ringenbach, J. C., Vauchez, A., Nalpas, T., et al. (2016). Basement-Cover decoupling and progressive exhumation of metamorphic sediments at hot rifted margin. Insights from the Northeastern Pyrenean analog. *Tectonophysics*, *686*, 82–97. https://doi.org/10.1016/j.tecto.2016.07.022

Clerc, C., Lagabrielle, Y., Neumaier, M., Reynaud, J.-Y., & de Saint Blanquat, M. (2012). Exhumation of subcontinental mantle rocks: Evidence from ultramafic-bearing clastic deposits nearby the Lherz peridotite body, French Pyrenees. *Bulletin de la Societe Geologique de France*, *183*(5), 443–459. https://doi.org/10.2113/gssgfbull.183.5.443

Clerc, C., Lahfid, A., Monié, P., Lagabrielle, Y., Chopin, C., Poujol, M., et al. (2015). High-temperature metamorphism during extreme thinning of the continental crust: A reappraisal of the North Pyrenean passive paleomargin. *Solid Earth*, *6*(2), 643–668. https://doi.org/10.5194/se-6-643-2015

Deckers, J. (2015). The Paleocene stratigraphic records in the Central Netherlands and close surrounding basins: Highlighting the different responses to a late Danian change in stress regime within the Central European Basin System. *Tectonophysics*, *659*, 102–108. https://doi.org/10.1016/J.TECTO.2015.07.031

de Bresser, J. H. P., ter Heege, J. H., & Spiers, C. J. (2001). Grain size reduction by dynamic recrystallization: Can it result in major rheological weakening? *International Journal of Earth Sciences*, *90*(1), 28–45. https://doi.org/10.1007/s005310000149

de Jager, J. (2003). Inverted basins in the Netherlands, similarities and differences. *Netherlands Journal of Geosciences*, *82*(4), 339–349. https://doi.org/10.1017/S0016774600020175

de Lugt, I. R., van Wees, J., & Wong, T. (2003). The tectonic evolution of the southern Dutch North Sea during the Palaeogene: Basin inversion in distinct pulses. *Tectonophysics*, *373*(1-4), 141–159. https://doi.org/10.1016/S0040-1951(03)00284-1

Deramond, J., Souquet, P., Fondecave-Wallez, M.-J., & Specht, M. (1993). Relationships between thrust tectonics and sequence stratigraphy surfaces in foredeeps: Model and examples from the Pyrenees (Cretaceous-Eocene, France, Spain). *Geological Society, London, Special Publications*, *71*(1), 193–219. https://doi.org/10.1144/GSL.SP.1993.071.01.09

de Saint Blanquat, M., Bajolet, F., Grand'Homme, A., Proietti, A., Zanti, M., Boutin, A., et al. (2016). Cretaceous mantle exhumation in the central Pyrenees: New constraints from the peridotites in eastern Ariège (North Pyrenean zone, France). *Comptes Rendus Geoscience*, *348*(3–4), 268–278. https://doi.org/10.1016/j.crte.2015.12.003

de Saint Blanquat, M., Lardeaux, J. M., & Brunel, M. (1990). Petrological arguments for high-temperature extensional deformation in the Pyrenean Variscan crust (Saint Barthélémy Massif, Ariège, France). *Tectonophysics*, *177*(1-3), 245–262. https://doi.org/10.1016/0040-1951(90)90284-F

Dewey, J. F., & Windley, B. F. (1988). Palaeocene-Oligocene tectonics of NW Europe. *Geological Society, London, Special Publications*, *39*(1), 25–31. https://doi.org/10.1144/GSL.SP.1988.039.01.04

Dèzes, P., Schmid, S. M., & Ziegler, P. A. (2004). Evolution of the European Cenozoic Rift System: Interaction of the Alpine and Pyrenean orogens with their foreland lithosphere. *Tectonophysics*, *389*(1-2), 1–33. https://doi.org/10.1016/j.tecto.2004.06.011

Diaz, J., Gallart, J., & Carbonell, R. (2016). Moho topography beneath the Iberian-Western Mediterranean region mapped from controlled-source and natural seismicity surveys. *Tectonophysics*, *692*, 74–85. https://doi.org/10.1016/j.tecto.2016.08.023

Diaz, J., Vergés, J., Chevrot, S., Antonio-Vigil, A., Ruiz, M., Sylvander, M., & Gallart, J. (2018). Mapping the crustal structure beneath the eastern Pyrenees. *Tectonophysics*, *744*, 296–309. https://doi.org/10.1016/j.tecto.2018.07.011

Dyksterhuis, S., & Müller, R. D. (2008). Cause and evolution of intraplate orogeny in Australia. *Geology*, *36*(6), 495–498. https://doi.org/10.1130/G24536A.1

Escartín, J., Hirth, G., & Evans, B. (2001). Strength of slightly serpentinized peridotites: Implications for the tectonics of oceanic lithosphere. *Geology*, *29*(11), 1023. https://doi.org/10.1130/0091-7613(2001)029<1023:SOSSPI>2.0.CO;2

Fernández-Viejo, G., Pulgar, J. A., Gallastegui, J., & Quintana, L. (2012). The fossil accretionary wedge of the Bay of Biscay: Critical wedge analysis on depth-migrated seismic sections and geodynamical implications. *The Journal of Geology*, *120*(3), 315–331. https://doi.org/10.1086/664789

Fischer, C., Dunkl, I., von Eynatten, H., Wijbrans, J. R., & Gaupp, R. (2012). Products and timing of diagenetic processes in Upper Rotliegend sandstones from Bebertal (North German Basin, Parchim Formation, Flechtingen High, Germany). *Geological Magazine*, *149*(5), 827–840. https://doi.org/10.1017/S0016756811001087

Ford, M., Hemmer, L., Vacherat, A., Gallagher, K., & Christophoul, F. (2016). Retro-wedge foreland basin evolution along the ECORS line, eastern Pyrenees, France. *Journal of the Geological Society*, *173*(3), 419–437. https://doi.org/10.1144/jgs2015-129

Fournier, F., Tassy, A., Thinon, I., Münch, P., Cornée, J.-J., Borgomano, J., et al. (2016). Pre-Pliocene tectonostratigraphic framework of the Provence continental shelf (eastern Gulf of Lion, SE France). *Bulletin de la Société Géologique de France*, *187*(4–5), 187–215. https://doi.org/10.2113/gssgfbull.187.4-5.187

Frasca, G., Gueydan, F., & Brun, J.-P. (2015). Structural record of Lower Miocene westward motion of the Alboran Domain in the Western Betics, Spain. *Tectonophysics*, *657*, 1–20. https://doi.org/10.1016/j.tecto.2015.05.017

Froitzheim, N., Stets, J., & Wurster, P. (1988). Aspects of Western High Atlas tectonics. In V. H. Jacobshagen (Ed.), *The Atlas System of Morocco: Studies on its Geodynamic Evolution* (pp. 219–244). Berlin, Heidelberg: Springer. https://doi.org/10.1007/BFb0011595

Gallart, J., Díaz, J., Nercessian, A., Mauffret, A., & Reis, T. D. (2001). The eastern end of the Pyrenees: Seismic features at the transition to the NW Mediterranean. *Geophysical Research Letters*, *28*(11), 2277–2280. https://doi.org/10.1029/2000GL012581

Gallastegui, J., Pulgar, J. A., & Gallart, J. (2002). Initiation of an active margin at the North Iberian continent-ocean transition. *Tectonics*, *21*(4), 1033. https://doi.org/10.1029/2001TC901046

Gleason, G. C., & Tullis, J. (1995). A flow law for dislocation creep of quartz aggregates determined with the molten salt cell. *Tectonophysics*, *247*(1-4), 1–23. https://doi.org/10.1016/0040-1951(95)00011-B

Grool, A. R., Ford, M., Vergés, J., Huismans, R. S., Christophoul, F., & Dielforder, A. (2018). Insights into the crustal-scale dynamics of a doubly vergent orogen from a quantitative analysis of its forelands: A case study of the Eastern Pyrenees. *Tectonics*, *37*, 450–476. https://doi.org/10.1002/2017TC004731

Guimerà, J., Mas, R., & Alonso, A. (2004). Intraplate deformation in the NW Iberian Chain: Mesozoic extension and Tertiary contractional inversion. *Journal of the Geological Society*, *161*(2), 291–303. https://doi.org/10.1144/0016-764903-055

Gunnell, Y., Zeyen, H., & Calvet, M. (2008). Geophysical evidence of a missing lithospheric root beneath the Eastern Pyrenees: Consequences for post-orogenic uplift and associated geomorphic signatures. *Earth and Planetary Science Letters*, *276*(3-4), 302–313. https://doi.org/10.1016/j.epsl.2008.09.031

Gurnis, M., Hall, C., & Lavier, L. (2004). Evolving force balance during incipient subduction. *Geochemistry, Geophysics, Geosystems*, *5*, Q07001. https://doi.org/10.1029/2003GC000681

Handy, M. R., Schmid, S. M., Bousquet, R., Kissling, E., & Bernoulli, D. (2010). Reconciling plate-tectonic reconstructions of Alpine Tethys with the geological-geophysical record of spreading and subduction in the Alps. *Earth-Science Reviews*, *102*(3-4), 121–158. https://doi.org/10.1016/j.earscirev.2010.06.002

Heidbach, O., Reinecker, J., Tingay, M., Müller, B., Sperner, B., Fuchs, K., & Wenzel, F. (2007). Plate boundary forces are not enough: Second- and third-order stress patterns highlighted in the World Stress Map database. *Tectonics*, *26*, TC6014. https://doi.org/10.1029/2007TC002133

Hirth, G., & Kohlstedt, D. (2003). Rheology of the upper mantle and the mantle wedge: A view from the experimentalists. In *Inside the Subduction Factory* (pp. 83–105). Washington, DC: American Geophysical Union. https://doi.org/10.1029/138GM06

Jammes, S., Manatschal, G., Lavier, L., & Masini, E. (2009). Tectonosedimentary evolution related to extreme crustal thinning ahead of a propagating ocean: Example of the western Pyrenees. *Tectonics*, *28*, TC4012. https://doi.org/10.1029/2008TC002406

Jones, C. H., Unruh, J. R., & Sonder, L. J. (1996). The role of gravitational potential energy in active deformation in the southwestern United States. *Nature*, *381*(6577), 37–41. https://doi.org/10.1038/381037a0

Jourdon, A., le Pourhiet, L., Mouthereau, F., & Masini, E. (2019). Role of rift maturity on the architecture and shortening distribution in mountain belts. *Earth and Planetary Science Letters*, *512*, 89–99. https://doi.org/10.1016/j.epsl.2019.01.057

Kley, J., Franzke, H.-J., Jähne, F., Krawczyk, C., Lohr, T., Reicherter, K., et al. (2008). Strain and Stress. In R. Littke, U. Bayer, D. Gajewski, & S. Nelskamp (Eds.), *Dynamics of Complex Intracontinental Basins—The Central European Basin System* (pp. 97–124). Berlin: Springer.

Kley, J., & Voigt, T. (2008). Late Cretaceous intraplate thrusting in central Europe: Effect of Africa-Iberia-Europe convergence, not Alpine collision. *Geology*, *36*(11), 839–842. https://doi.org/10.1130/G24930A.1

Kockel, F. (2003). Inversion structures in Central Europe—Expressions and reasons, an open discussion. *Netherlands Journal of Geosciences*, *82*(4), 351–366. https://doi.org/10.1017/S0016774600020187

Krzywiec, P. (2006). Structural inversion of the Pomeranian and Kuiavian segments of the Mid-Polish Trough—Lateral variations in timing and structural style. *Geological Quarterly*, *50*(1), 151–168.

Labaume, P., Meresse, F., Jolivet, M., Teixell, A., & Lahfid, A. (2016). Tectonothermal history of an exhumed thrust-sheet-top basin: An example from the south Pyrenean thrust belt. *Tectonics*, *35*, 1280–1313. https://doi.org/10.1002/2016TC004192

Lacombe, O., & Jolivet, L. (2005). Structural and kinematic relationships between Corsica and the Pyrenees-Provence domain at the time of the Pyrenean orogeny. *Tectonics*, *24*, TC1003. https://doi.org/10.1029/2004TC001673

Lagabrielle, Y., Labaume, P., & de Saint Blanquat, M. (2010). Mantle exhumation, crustal denudation, and gravity tectonics during Cretaceous rifting in the Pyrenean realm (SW Europe): Insights from the geological setting of the lherzolite bodies. *Tectonics*, *29*, TC4012. https://doi.org/10.1029/2009TC002588

Lamb, S. (2006). Shear stresses on megathrusts: Implications for mountain building behind subduction zones. *Journal of Geophysical Research*, *111*, B07401. https://doi.org/10.1029/2005JB003916

Leleu, S., Ghienne, J.-F., & Manatschal, G. (2009). Alluvial fan development and morpho-tectonic evolution in response to contractional fault reactivation (Late Cretaceous–Palaeocene), Provence, France. *Basin Research*, *21*(2), 157–187. https://doi.org/10.1111/j.1365-2117.2008.00378.x

Levandowski, W., Herrmann, R. B., Briggs, R., Boyd, O., & Gold, R. (2018). An updated stress map of the continental United States reveals heterogeneous intraplate stress. *Nature Geoscience*, *11*(6), 433–437. https://doi.org/10.1038/s41561-018-0120-x

Littke, R., Scheck-Wenderoth, M., Brix, M. R., & Nelskamp, S. (2008). Subsidence, inversion and evolution of the thermal field. In R. Littke, U. Bayer, D. Gajewski, & S. Nelskamp (Eds.), *Dynamics of Complex Intracontinental Basins—The Central European Basin System* (pp. 125–153). Berlin: Springer.

Lohr, T., Krawczyk, C. M., Tanner, D. C., Samiee, R., Endres, H., Oncken, O., et al. (2007). Strain partitioning due to salt: Insights from interpretation of a 3D seismic data set in the NW German Basin. *Basin Research*, *19*(4), 579–597. https://doi.org/10.1111/j.1365-2117.2007.00338.x

Macchiavelli, C., Vergés, J., Schettino, A., Fernàndez, M., Turco, E., Casciello, E., et al. (2017). A new southern North Atlantic isochron map: Insights into the drift of the Iberian Plate since the Late Cretaceous. *Journal of Geophysical Research: Solid Earth*, *122*, 9603–9626. https://doi.org/10.1002/2017JB014769

Marotta, A. ., Bayer, U., Thybo, H., & Scheck, M. (2002). Origin of the regional stress in the North German basin: Results from numerical modelling. *Tectonophysics*, *360*(1-4), 245–264. https://doi.org/10.1016/S0040-1951(02)00358-X

Masini, E., Manatschal, G., Tugend, J., Mohn, G., & Flament, J.-M. (2014). The tectono-sedimentary evolution of a hyper-extended rift basin: the example of the Arzacq–Mauléon rift system (Western Pyrenees, SW France). *International Journal of Earth Sciences*, *103*(6), 1569–1596. https://doi.org/10.1007/s00531-014-1023-8

Matysiak, A. K., & Trepmann, C. A. (2015). The deformation record of olivine in mylonitic peridotites from the Finero Complex, Ivrea Zone: Separate deformation cycles during exhumation. *Tectonics*, *34*, 2514–2533. https://doi.org/10.1002/2015TC003904

Mauffret, A., & Gorini, C. (1996). Structural style and geodynamic evolution of Camargue and Western Provencal basin, southeastern France. *Tectonics*, *15*(2), 356–375. https://doi.org/10.1029/95TC02407

McClay, K., Munoz, J. A., & García-Senz, J. (2004). Extensional salt tectonics in a contractional orogen: A newly identified tectonic event in the Spanish Pyrenees. *Geology*, *32*(9), 737–740. https://doi.org/10.1130/G20565.1

Metcalf, J. R., Fitzgerald, P. G., Baldwin, S. L., & Muñoz, J.-A. (2009). Thermochronology of a convergent orogen: Constraints on the timing of thrust faulting and subsequent exhumation of the Maladeta Pluton in the Central Pyrenean Axial Zone. *Earth and Planetary Science Letters*, *287*(3-4), 488–503. https://doi.org/10.1016/j.epsl.2009.08.036

Molnar, P., & England, P. (1990). Temperatures, heat flux, and frictional stress near major thrust faults. *Journal of Geophysical Research*, *95*(B4), 4833–4856. https://doi.org/10.1029/JB095iB04p04833

Moore, D. E., Lockner, D. A., Ma, S., Summers, R., & Byerlee, J. D. (1997). Strengths of serpentinite gouges at elevated temperatures. *Journal of Geophysical Research*, *102*(B7), 14,787–14,801. https://doi.org/10.1029/97JB00995

Mouthereau, F., Filleaudeau, P.-Y., Vacherat, A., Pik, R., Lacombe, O., Fellin, M. G., et al. (2014). Placing limits to shortening evolution in the Pyrenees: Role of margin architecture and implications for the Iberia/Europe convergence. *Tectonics*, *33*, 2283–2314. https://doi.org/10.1002/2014TC003663

Muñoz, J. A. (1992). Evolution of a continental collision belt: ECORS-Pyrenees crustal balanced cross-section BT—Thrust Tectonics. In K. R. McClay (Ed.) (pp. 235–246). Dordrecht, Netherlands: Springer. https://doi.org/10.1007/978-94-011-3066-0_21

Navabpour, P., Malz, A., Kley, J., Siegburg, M., Kasch, N., & Ustaszewski, K. (2017). Intraplate brittle deformation and states of paleostress constrained by fault kinematics in the central German platform. *Tectonophysics*, *694*, 146–163. https://doi.org/10.1016/j.tecto.2016.11.033

Nielsen, S. B., & Hansen, D. L. (2000). Physical explanation of the formation and evolution of inversion zones and marginal troughs. *Geology*, *28*(10), 875–878. https://doi.org/10.1130/0091-7613(2000)28<875:PEOTFA>2.0.CO;2

Nielsen, S. B., Stephenson, R., & Thomsen, E. (2007). Dynamics of Mid-Palaeocene North Atlantic rifting linked with European intra-plate deformations. *Nature*, *450*(7172), 1071–1074. https://doi.org/10.1038/nature06379

Nielsen, S. B., Thomsen, E., Hansen, D. L., & Clausen, O. R. (2005). Plate-wide stress relaxation explains European Palaeocene basin inversions. *Nature*, *435*(7039), 195–198. https://doi.org/10.1038/nature03599

Nirrengarten, M., Manatschal, G., Tugend, J., Kusznir, N. J., & Sauter, D. (2018). Kinematic evolution of the s outhern North Atlantic: Implications for the formation of hyperextended rift systems. *Tectonics*, *37*, 89–118. https://doi.org/10.1002/2017TC004495

Pedreira, D., Afonso, J. C., Pulgar, J. A., Gallastegui, J., Carballo, A., Fernàndez, M., et al. (2015). Geophysical-petrological modeling of the lithosphere beneath the Cantabrian Mountains and the North-Iberian margin: geodynamic implications. *Lithos*, *230*, 46–68. https://doi.org/10.1016/j.lithos.2015.04.018

Pedreira, D., Pulgar, J. A., Gallart, J., & Díaz, J. (2003). Seismic evidence of Alpine crustal thickening and wedging from the western Pyrenees to the Cantabrian Mountains (north Iberia). *Journal of Geophysical Research*, *108*(B4), 2204. https://doi.org/10.1029/2001JB001667

Pedreira, D., Pulgar, J. A., Gallart, J., & Torné, M. (2007). Three-dimensional gravity and magnetic modeling of crustal indentation and wedging in the western Pyrenees-Cantabrian Mountains. *Journal of Geophysical Research*, *112*, B12405. https://doi.org/10.1029/2007JB005021

Pfiffner, O. A., Schlunegger, F., & Buiter, S. J. H. (2002). The Swiss Alps and their peripheral foreland basin: Stratigraphic response to deep crustal processes. *Tectonics*, *21*(2), 1009. https://doi.org/10.1029/2000TC900039

Popov, A. A., & Sobolev, S. V. (2008). SLIM3D: A tool for three-dimensional thermomechanical modeling of lithospheric deformation with elasto-visco-plastic rheology. *Physics of the Earth and Planetary Interiors*, *171*(1-4), 55–75. https://doi.org/10.1016/J.PEPI.2008.03.007

Raimondo, T., Hand, M., & Collins, W. J. (2014). Compressional intracontinental orogens: Ancient and modern perspectives. *Earth-Science Reviews*, *130*, 128–153. https://doi.org/10.1016/j.earscirev.2013.11.009

Reicherter, K. R., & Pletsch, T. K. (2000). Evidence for a synchronous circum-Iberian subsidence event and its relation to the African-Iberian plate convergence in the Late Cretaceous. *Terra Nova*, *12*(3), 141–147. https://doi.org/10.1046/j.1365-3121.2000.123276.x

Roca, E., Muñoz, J. A., Ferrer, O., & Ellouz, N. (2011). The role of the Bay of Biscay Mesozoic extensional structure in the configuration of the Pyrenean orogen: Constraints from the MARCONI deep seismic reflection survey. *Tectonics*, *30*, TC2001. https://doi.org/10.1029/2010TC002735

Rosenbaum, G., Lister, G. S., & Duboz, C. (2002). Relative motions of Africa, Iberia and Europe during Alpine orogeny. *Tectonophysics*, *359*(1–2), 117–129. https://doi.org/10.1016/S0040-1951(02)00442-0

Rougier, G., Ford, M., Christophoul, F., & Bader, A.-G. (2016). Stratigraphic and tectonic studies in the central Aquitaine Basin, northern Pyrenees: Constraints on the subsidence and deformation history of a retro-foreland basin. *Comptes Rendus Geoscience*, *348*(3-4), 224–235. https://doi.org/10.1016/j.crte.2015.12.005

Roure, F., Choukroune, P., Berastegui, X., Munoz, J. A., Villien, A., Matheron, P., et al. (1989). Ecors deep seismic data and balanced cross sections: Geometric constraints on the evolution of the Pyrenees. *Tectonics*, *8*(1), 41–50. https://doi.org/10.1029/TC008i001p00041

Ruiz, M., Díaz, J., Pedreira, D., Gallart, J., & Pulgar, J. A. (2017). Crustal structure of the North Iberian continental margin from seismic refraction/wide-angle reflection profiles. *Tectonophysics*, *717*, 65–82. https://doi.org/10.1016/j.tecto.2017.07.008

Sainz, C. A. M., & Faccenna, C. (2001). Tertiary compressional deformation of the Iberian plate. *Terra Nova*, *13*(4), 281–288. https://doi.org/10.1046/j.1365-3121.2001.00355.x

Sandiford, M. (1999). Mechanics of basin inversion. *Tectonophysics*, *305*(1-3), 109–120. https://doi.org/10.1016/S0040-1951(99)00023-2

Scheck-Wenderoth, M., & Lamarche, J. (2005). Crustal memory and basin evolution in the Central European Basin System—new insights from a 3D structural model. *Tectonophysics*, *397*(1–2), 143–165. https://doi.org/10.1016/j.tecto.2004.10.007

Schettino, A., & Turco, E. (2011). Tectonic history of the western Tethys since the Late Triassic. *Geological Society of America Bulletin*, *123*(1–2), 89–105. https://doi.org/10.1130/B30064.1

Schumacher, M. E. (2002). Upper Rhine Graben: Role of preexisting structures during rift evolution. *Tectonics*, *21*(1), 1006. https://doi.org/10.1029/2001TC900022

Senglaub, Y., Brix, M. R., Adriasola, A. C., & Littke, R. (2005). New information on the thermal history of the southwestern Lower Saxony Basin, northern Germany, based on fission track analysis. *International Journal of Earth Sciences*, *94*(5-6), 876–896. https://doi.org/10.1007/s00531-005-0008-z

Senglaub, Y., Littke, R., & Brix, M. R. (2006). Numerical modelling of burial and temperature history as an approach for an alternative interpretation of the Bramsche anomaly, Lower Saxony Basin. *International Journal of Earth Sciences*, *95*(2), 204–224. https://doi.org/10.1007/s00531-005-0033-y

Séranne, M. (1999). The Gulf of Lion continental margin (NW Mediterranean) revisited by IBS: an overview. *Geological Society, London, Special Publications*, *156*(1), 15–36. https://doi.org/10.1144/GSL.SP.1999.156.01.03

Sibuet, J.-C., & Collette, B. J. (1991). Triple junctions of Bay of Biscay and North Atlantic: New constraints on the kinematic evolution. *Geology*, *19*(5), 522–525. https://doi.org/10.1130/0091-7613(1991)019<0522:TJOBOB>2.3.CO;2

Sibuet, J.-C., Srivastava, S. P., & Spakman, W. (2004). Pyrenean orogeny and plate kinematics. *Journal of Geophysical Research*, *109*, B08104. https://doi.org/10.1029/2003JB002514

Sinclair, H. D. (2005). Asymmetric growth of the Pyrenees revealed through measurement and modeling of orogenic fluxes. *American Journal of Science*, *305*(5), 369–406. https://doi.org/10.2475/ajs.305.5.369

Sippel, J., Reicherter, K., & Mazur, S. (2009). Paleostress states at the south-western margin of the Central European Basin System—Application of fault-slip analysis to unravel a polyphase deformation pattern. *Tectonophysics*, *470*(1–2), 129–146. https://doi.org/10.1016/J.TECTO.2008.04.010

Stampfli, G. M., Mosar, J., Marquer, D., Marchant, R., Baudin, T., & Borel, G. (1998). Subduction and obduction processes in the Swiss Alps. *Tectonophysics*, *296*(1-2), 159–204. https://doi.org/10.1016/S0040-1951(98)00142-5

Stern, R. J. (2004). Subduction initiation: Spontaneous and induced. *Earth and Planetary Science Letters*, *226*(3-4), 275–292. https://doi.org/10.1016/j.epsl.2004.08.007

Stüwe, K. (2007). *Geodynamics of the Lithosphere: An Introduction. Geodynamics of the Lithosphere: An Introduction*. Berlin Heidelberg: Springer. https://doi.org/10.1007/978-3-540-71237-4

Sutherland, R., Collot, J., Bache, F., Henrys, S., Barker, D., Browne, G. H., et al. (2017). Widespread compression associated with Eocene Tonga-Kermadec subduction initiation. *Geology*, *45*(4), 355–358. https://doi.org/10.1130/G38617.1

Tanner, D. C., & Krawczyk, C. M. (2017). Restoration of the Cretaceous uplift of the Harz Mountains, North Germany: Evidence for the geometry of a thick-skinned thrust. *International Journal of Earth Sciences*, *106*(8), 2963–2972. https://doi.org/10.1007/s00531-017-1475-8

Tavani, S., Bertok, C., Granado, P., Piana, F., Salas, R., Vigna, B., & Muñoz, J. A. (2018). The Iberia-Eurasia plate boundary east of the Pyrenees. *Earth-Science Reviews*, *187*, 314–337. https://doi.org/10.1016/J.EARSCIREV.2018.10.008

Teixell, A., Labaume, P., Ayarza, P., Espurt, N., de Saint Blanquat, M., & Lagabrielle, Y. (2018). Crustal structure and evolution of the Pyrenean-Cantabrian belt: A review and new interpretations from recent concepts and data. *Tectonophysics*, *724-725*, 146–170. https://doi.org/10.1016/j.tecto.2018.01.009

Ternois, S., Odlum, M., Ford, M., Pik, R., Stockli, D., Tibari, B., et al. (2019). Thermochronological evidence of early orogenesis, eastern Pyrenees, France. *Tectonics*, *38*, 1308–1336. https://doi.org/10.1029/2018TC005254

Thomson, S. N., & Zeh, A. (2000). Fission-track thermochronology of the Ruhla Crystalline Complex: New constraints on the post-Variscan thermal evolution of the NW Saxo-Bohemian Massif. *Tectonophysics*, *324*(1-2), 17–35. https://doi.org/10.1016/S0040-1951(00)00113-X

Torsvik, T. H., Müller, R. D., van der Voo, R., Steinberger, B., & Gaina, C. (2008). Global plate motion frames: Toward a unified model. *Reviews of Geophysics*, *46*, RG3004. https://doi.org/10.1029/2007RG000227

Trepmann, C. A., Renner, J., & Druiventak, A. (2013). Experimental deformation and recrystallization of olivine-processes and time-scales of damage healing during postseismic relaxation at mantle depths. *Solid Earth*, *4*(2), 423–450. https://doi.org/10.5194/se-4-423-2013

Tugend, J., Manatschal, G., & Kusznir, N. J. (2015). Spatial and temporal evolution of hyperextended rift systems: Implication for the nature, kinematics, and timing of the Iberian-European plate boundary. *Geology*, *43*(1), 15–18. https://doi.org/10.1130/G36072.1

Tugend, J., Manatschal, G., Kusznir, N. J., Masini, E., Mohn, G., & Thinon, I. (2014). Formation and deformation of hyperextended rift systems: Insights from rift domain mapping in the Bay of Biscay-Pyrenees. *Tectonics*, *33*, 1239–1276. https://doi.org/10.1002/2014TC003529

Turner, J. P., & Williams, G. A. (2004). Sedimentary basin inversion and intra-plate shortening. *Earth-Science Reviews*, *65*(3–4), 277–304. https://doi.org/10.1016/J.EARSCIREV.2003.10.002

Vacherat, A., Mouthereau, F., Pik, R., Bernet, M., Gautheron, C., Masini, E., et al. (2014). Thermal imprint of rift-related processes in orogens as recorded in the Pyrenees. *Earth and Planetary Science Letters*, *408*, 296–306. https://doi.org/10.1016/j.epsl.2014.10.014

Vacherat, A., Mouthereau, F., Pik, R., Huyghe, D., Paquette, J.-L., Christophoul, F., et al. (2017). Rift-to-collision sediment routing in the Pyrenees: A synthesis from sedimentological, geochronological and kinematic constraints. *Earth-Science Reviews*, *172*, 43–74. https://doi.org/10.1016/j.earscirev.2017.07.004

van den Beukel, J. (1992). Some thermomechanical aspects of the subduction of continental lithosphere. *Tectonics*, *11*(2), 316–329. https://doi.org/10.1029/91TC01039

Vejbæk, O. V., & Andersen, C. (2002). Post mid-Cretaceous inversion tectonics in the Danish Central Graben: Regionally synchronous tectonic events? *Bulletin of the Geological Society of Denmark*, *49*, 129–144.

Vergés, J., & Fernàndez, M. (2012). Tethys–Atlantic interaction along the Iberia–Africa plate boundary: The Betic–Rif orogenic system. *Tectonophysics*, *579*, 144–172. https://doi.org/10.1016/J.TECTO.2012.08.032

Vergés, J., Fernàndez, M., & Martìnez, A. (2002). The Pyrenean orogen: Pre-, syn-, and post-collisional evolution. *Journal of the Virtual Explorer*, *08*, 55–74. https://doi.org/10.3809/jvirtex.2002.00058

Vergés, J., Millán, H., Roca, E., Muñoz, J. A., Marzo, M., Cirés, J., et al. (1995). Eastern Pyrenees and related foreland basins: Pre-, syn- and post-collisional crustal-scale cross-sections. *Marine and Petroleum Geology*, *12*(8), 903–915. https://doi.org/10.1016/0264-8172(95)98854-X

Vissers, R. L. M., & Meijer, P. T. (2012). Iberian plate kinematics and Alpine collision in the Pyrenees. *Earth-Science Reviews*, *114*(1–2), 61–83. https://doi.org/10.1016/j.earscirev.2012.05.001

von Eynatten, H., Voigt, T., Meier, A., Franzke, H.-J., & Gaupp, R. (2008). Provenance of Cretaceous clastics in the Subhercynian Basin: Constraints to exhumation of the Harz Mountains and timing of inversion tectonics in Central Europe. *International Journal of Earth Sciences*, *97*(6), 1315–1330. https://doi.org/10.1007/s00531-007-0212-0

Wagreich, M. (1995). Subduction tectonic erosion and Late Cretaceous subsidence along the northern Austroalpine margin (Eastern Alps, Austria). *Tectonophysics*, *242*(1–2), 63–78. https://doi.org/10.1016/0040-1951(94)00151-X

Wang, K., & He, J. (1999). Mechanics of low-stress forearcs: Nankai and Cascadia. *Journal of Geophysical Research*, *104*(B7), 15,191–15,205. https://doi.org/10.1029/1999JB900103

Yelland, A. J. (1991). *Thermo-Tectonics of the Pyrenees and Provence from Fission Track Studies*. London: Birbeck College, University of London.

Ziegler, P. A. (1987). Late Cretaceous and Cenozoic intra-plate compressional deformations in the Alpine foreland—A geodynamic model. *Tectonophysics*, *137*(1-4), 389–420. https://doi.org/10.1016/0040-1951(87)90330-1

Ziegler, P. A., Cloetingh, S., & van Wees, J.-D. (1995). Dynamics of intra-plate compressional deformation: The Alpine foreland and other examples. *Tectonophysics*, *252*(1-4), 7–59. https://doi.org/10.1016/0040-1951(95)00102-6

Zoback, M. L. (1992). First- and second-order patterns of stress in the lithosphere: The World Stress Map Project. *Journal of Geophysical Research*, *97*(B8), 11,703–11,728. https://doi.org/10.1029/92JB00132

Zoback, M. L., & Zoback, M. D. (1989). Chapter 24: Tectonic stress field of the continental United States. In L. C. Pakiser & W. D. Mooney (Eds.), *Geophysical Framework of the Continental United States* (pp. 523–540). Boulder: Geological Society of America. https://doi.org/10.1130/MEM172-p523